10.1161/CIRCULATIONAHA.116.025722

# SOX17 Regulates Conversion of Human Fibroblasts into Endothelial Cells and Erythroblasts via De-Differentiation into CD34$^+$ Progenitor Cells

**Running Title:** *Zhang et al.; SOX17 Regulation of Endothelial Lineage Conversion*

Lianghui Zhang, MD, PhD[1]; Ankit Jambusaria, BA[1]; Zhigang Hong, MD[1]; Glenn Marsboom, PhD[1]; Peter T. Toth, PhD[1]; Brittney-Shea Herbert, PhD[2]; Asrar B. Malik, PhD[1]; Jalees Rehman, MD[1,3]

[1]Department of Pharmacology, the University of Illinois College of Medicine, Chicago, IL; [2] Department of Medical and Molecular Genetics, Indiana University School of Medicine, Indianapolis, IN; [3] Department of Medicine, Division of Cardiology, the University of Illinois College of Medicine, Chicago, IL

**Address for Correspondence:**
Jalees Rehman, MD or Asrar B. Malik, PhD
The University of Illinois College of Medicine
835 South Wolcott Avenue, RM. E403
Mailcode 868, Chicago, IL 60612
Tel: 312-996-5552
Fax: 312-996-1225
Email: jalees@uic.edu
or abmalik@uic.edu

**Journal Subject Terms:** Angiogenesis; Cell Signalling/Signal Transduction; Cell Therapy; Cellular Reprogramming; Vascular Biology

## Abstract

***Background*—**The mechanisms underlying the de-differentiation and lineage conversion of adult human fibroblasts into functional endothelial cells have not yet been fully defined. Furthermore, it is not known whether fibroblast de-differentiation recapitulates the generation of multipotent progenitors during embryonic development which give rise to endothelial and hematopoietic cell lineages. Here we established the role of the developmental transcription factor SOX17 in regulating the bi-lineage conversion of fibroblasts via the generation of intermediate progenitors.
***Methods***—$CD34^+$ progenitors were generated following the de-differentiation of human adult dermal fibroblasts by overexpression of pluripotency transcription factors. Sorted $CD34^+$ cells were transdifferentiated into induced endothelial cells (iECs) and induced erythroblasts (iErythroblasts) using lineage specific growth factors. The therapeutic potential of the generated cells was assessed in an experimental model of myocardial infarction.
***Results*—**iECs expressed specific endothelial cell surface markers and also exhibited the capacity for cell proliferation and neovascularization. Induced erythroblasts expressed erythroid surface markers and formed erythroid colonies. Endothelial lineage conversion was dependent on the upregulation of the developmental transcription factor SOX17 whereas suppression of SOX17 instead directed the cells towards an erythroid fate. Implantation of these human bi-potential $CD34^+$ progenitors into immune-deficient NOD-SCID mice resulted in the formation of micro-vessels derived from human endothelial cells that were perfused with mouse and human erythrocytes. iECs generated from human fibroblasts showed upregulation of telomerase. Cell implantation markedly improved vascularity and cardiac function after myocardial infarction without any evidence of teratoma formation.
***Conclusions***—De-differentiation of fibroblasts to intermediate $CD34^+$ progenitors gives rise to endothelial cells and erythroblasts in a SOX17-dependent manner. These findings identify the intermediate $CD34^+$ progenitor state as a critical bifurcation point which can be tuned to generate functional blood vessels or erythrocytes and salvage ischemic tissue.


**Key-Words:** progenitor cell; transcriptional regulation; regeneration; endothelial cell differentiation; fibroblasts; reprogramming, erythroblasts, erythropoiesis, vascular biology

## Clinical Perspective

### What is new?

- Adult human skin fibroblasts can be de-differentiated to intermediate $CD34^+$ progenitors which in turn give rise to endothelial cells as well as erythrocytes
- Lineage conversion of fibroblasts via partial de-differentiation recapitulates in part the embryonic development of the vasculature as evidenced by upregulation of the anti-aging enzyme telomerase and the bi-lineage potential of the generated progenitors.
- The transcription factor SOX17 functions as a switch which regulates cell fate of $CD34^+$ progenitors towards an endothelial versus erythroid lineage.
- Implanted fibroblast-derived $CD34^+$ progenitors stably engraft to form functional human blood vessels in mice that improve cardiac function after myocardial infarction.

### What are the clinical implications?

- De-differentiation of fibroblasts to multipotent progenitors can generate patient-specific functional endothelial cells
- When human fibroblast-derived progenitors are implanted in a mouse model of myocardial infarction, they are able to improve cardiac function
- The molecular switch SOX17 provides a means to optimize the generation of endothelial cells for vascular tissue regeneration or disease modeling
- The upregulation of telomerase suggests that fibroblast de-differentiation may avoid premature aging of the cells during the lineage conversion process which could be especially helpful when deriving personalized endothelial cells from skin fibroblasts of older patients

## Introduction

Direct conversion of somatic cells such as fibroblasts into other cell types for organ and tissue regeneration holds great therapeutic promise [1]. Studies have shown that fibroblasts can be re-programmed into hepatocyte-like cells, cardiomyocytes, neurons, endothelial cells (ECs), and erythroid progenitors[2-6]. Direct conversion of fibroblasts to regenerative therapeutic cells is thus not only more expedient than the intermediate generation of iPSCs which requires further differentiation into specific lineage cells but also avoids risk of teratoma formation caused by any residual pluripotent cells[7]. Two general strategies are used to convert fibroblasts into ECs. One relies on de-differentiation in which the pluripotency-inducing transcription factors OCT-4, KLF4, SOX2, and c-MYC are expressed to partially de-differentiate fibroblasts, and this is followed by applying endothelial growth factors such as VEGF to induce terminal EC differentiation[8-10]. The second approach relies on the targeted over-expression of developmental transcription factors, such as ETV2, known to regulate formation of ECs[11, 12].

However, little is known about the underlying mechanisms which enable reprogramming and whether these two strategies – partial de-differentiation and directed vascular transcription factor over-expression – can be combined. The advantage of the de-differentiation strategy is that it may generate multipotent progenitors which can in turn be directed into multiple regenerative cell lineages. ECs generated during embryonic development are derived from mesodermal progenitors, hemangioblasts, which are a short-lived cell population that generates both endothelial and hematopoietic lineage cells[13-15]. Thus, we surmised that if de-differentiation of adult fibroblasts recapitulates embryonic development then generation of fibroblast-derived progenitors may also provide a means of forming new blood vessels along with hematopoietic cells including erythrocytes. Human hemangioblasts reportedly have distinct sub-populations

expressing different surface markers such as CD34[16-18]. Here we demonstrated that de-differentiation of human fibroblasts generated bipotential $CD34^+$ progenitors, capable of differentiating into ECs and erythroblasts. The transcription factor SOX17 functioned as a tunable rheostat-like switch in $CD34^+$ cells giving rise to ECs and the erythroid lineage. Further, we demonstrated that implantation of $CD34^+$ progenitors generated functional human blood vessels and improved cardiac function in infarcted mouse hearts.

## Methods

### Cell culture and transfection

Normal human adult dermal fibroblast cells (Lonza, CC-2511) and human neonatal dermal fibroblast cells (Lonza, CC-2509) were cultured in DMEM (Life Technologies, 21063) containing 10% FBS, 50 U/ml penicillin and 50 mg/ml streptomycin, 2.25mM each L-glutamine and non-essential amino acids. Fibroblasts ($5.0\times10^5$/100mm dish) and PLAT-A cells (Cell Biolabs Inc. RV-102) ($5.0\times10^6$/100mm dish) were plated in DMEM medium without antibiotics. 100 mm dishes were plated with PLAT-A cells, one dish per plasmid – each encoding OCT4, KLF4, SOX2, and c-MYC (OKSM – all obtained from Addgene), as well as GFP as a control. On Day 0, Fugene HD transfection reagent (Roche, E2311) and 10μg of the appropriate plasmid DNA were added to one 100 mm dish cultured with PLAT-A cells. The virus-containing medium was collected and filtered from dishes of transfected PLAT-A cells on Day 1 and Day 2 for titration. The medium of human fibroblasts was replaced with virus-containing medium on Day 1 and Day 2. On Day 3, the medium was switched to DMEM/F12 (Life Technologies, 11330), 20% KnockOut serum replacement (Life Technologies, 10828), 10ng $ml^{-1}$ bFGF (R&D Systems, 233-FB), 1mM GlutaMAX, 0.1mM non-essential amino acids, and 55μM β-mercaptoethanol

with medium changes every day for 5 days to continue the de-differentiation phase. The fibroblasts transduced by OKSM and maintained in this medium were referred to as de-differentiated fibroblasts (De-Diff-Fib). The protocol is shown in Figure 1A. All cell lines were maintained in an incubator (37℃, 5% $CO_2$).

**Isolation of CD34$^+$ progenitors from de-differentiated fibroblasts**

We identified the CD34$^+$ progenitors by CD34, a marker of human progenitors, including endothelial progenitors and hematopoietic progenitors[18]. We isolated CD34$^+$ cells generated during de-differentiation of fibroblast with anti-CD34–conjugated magnetic beads (Miltenyi, 130-046) according to manufacturer's instructions with slight modifications. Briefly, up to $10^9$ cells were incubated at 4°C with 100µl of Fc-blocking solution and 100µl anti-CD34 magnetic beads in a total volume of 500µl FACS blocking buffer. After 30 min, cells were sorted by 2 consecutive rounds of column separation through applying MACS separation magnets to increase purity.

**Differentiation of CD34$^+$ progenitors into iECs**

Isolated CD34$^+$ progenitors were plated in 0.1% gelatin–coated plates ($2 \times 10^5$/6-well) and cultured in endothelial medium EGM-2 (CC-4176), supplemented with 50ng/ml BMP4 (R&D Systems, 314-BP) and 50ng/ml VEGF (R&D Systems, 293-VE) to induce endothelial lineage specification and the medium was changed every other day. Upon reaching ~90% confluence, cells were split 1:3. Primary human aortic ECs were purchased from Lonza (CC-2535) and cultured in EGM-2 medium as control cells.

**Differentiation of CD34$^+$ progenitors into iErythroblasts**

To generate erythroid cells, sorted CD34$^+$ progenitors were plated in 0.1% gelatin–coated plates ($1.0\times10^6$/well in a 6-well plate) and cultured for 4 days in erythroblast induction medium which

consisted of 49% IMDM (Life technologies, 12440), 49% Ham's F12 (Life technologies, 11765), 1% ITSX, 1% lipid (Life technologies, 11905-031), 5mg/100ml I-ascorbic acid (Sigma, A8960), 500mg/100ml BSA (Sigma, A7030), and 200uM 1-thioglycerol (Sigma, M6145), supplemented with 100ng/ml SCF (PeproTech, 300-07), 10ng/ml IL-3 (PeproTech, 200-03), 5U/ml EPO (R&D systems, 287-TC), 40ng/ml IGF-1(Sigma I-3769), 1 μM Dexamethsone (Sigma, D2915), 50ng/ml Flt3-L(PeproTech, 300-19) (Figure 1A). Unlike adherent ECs, iErythroblasts detached upon generation and were collected as non-adherent cell fraction at Day 4 for characterization.

**Matrigel plug in vivo angiogenesis assay**

To test the ability of iECs to form blood vessels in vivo, we performed an in vivo gel plug assay[19]. Immune-deficient NOD-SCID mice were used to avoid the rejection of human cells. Anesthesia was induced using a mixture of xylazine (10mg/kg) and ketamine (100mg/kg) in saline i.p. A total of $1\times10^6$ cells (either $CD34^+$ progenitors, fibroblasts or aortic ECs) were suspended in 200μl of cold growth-factor reduced Matrigel Matrix (Corning, 356234). We then injected the cell-containing Matrigel solutions subcutaneously in the abdomen. The mice were sacrificed after one week implantation and the Matrigel plugs were removed by a wide excision of the skin, fixed in 10% formalin overnight, embedded in paraffin and sectioned. Five sections from each plug were randomly selected to quantify human vessels. Quantification of vessel density in angiogenesis plugs was shown per section per plug. Each mouse was injected with three plugs containing either iECs, fibroblasts or mature ECs. Each data point represents one plug from one mice.

**Myocardial infarction surgery and intramyocardial injection of cells**

The myocardial infarction surgery is described in detail in the Supplemental Material. For the cell implantation, 40 μl of concentrated cells - $1\times10^6$ $CD34^+$ progenitors or fibroblasts suspended

in growth-factor reduced Matrigel (Matrigel basement-membrane matrix from BD) were injected into the border zone of the infarct at 2-3 different areas using a Gastight 1710 syringe (Hamilton) immediately after ligation. The injected cells had been pre-labeled with lentiviral GFP. The surgeon was blinded to the nature of the injected cells. Two weeks later, hearts were retrograde perfused with 4% paraformaldehyde via the aorta, fixed in 4% paraformaldehyde for 4 hours, incubated in 30% sucrose overnight, embedded in OCT, frozen, and cryosectioned. Ten sections with injected GFP cells from each heart were used for quantification of human CD31+ vessels. Quantification of vessel density was shown as vessels per section per heart.

**Experimental animals**

Immune-deficient NOD-SCID mice were purchased from Jackson Laboratory (NOD.Cg-*Prkdc*$^{scid}$ *Il2rg*$^{tm1Wjl}$/SzJ, strain 005557). All animal experiments were conducted in accordance with NIH guidelines for the care and use of live animals and were approved by the IACUC of the University of Illinois.

**Statistics**

Cell culture studies on fibroblasts and endothelial cells were performed with commercially obtained primary cells from multiple batches (Lonza) and are biological replicates. Values were reported as mean±SE. The statistical analysis was performed with GraphPad Prism and is indicated in the figure legends. Bonferroni corrections were used for ANOVA with multiple comparisons. Statistical significance was set at $p<0.05$.

**Results**

**De-differentiation of human fibroblasts into CD34$^+$ progenitors**

CD34$^+$ progenitors were generated by expressing the "Yamanaka" factors OCT4, KLF4, SOX2,

and c-MYC (OKSM) in human fibroblasts followed by 7 days of de-differentiation (Figure 1A). These fibroblast-derived cells were referred to as de-differentiated fibroblasts (De-Diff-Fib), and we subsequently applied endothelial or erythroid lineage growth factors to differentiate them into ECs or erythroblasts (Figure 1A and Supplemental Figure 1). As shown in Figure 1B, expression of *CD34* gradually increased during the de-differentiation period and reached a plateau at Day 6-7. *OCT4* mRNA levels peaked at Day 3 to Day 4 and then steadily decreased (Figure 1C), indicating that pluripotency was circumvented. Expression of *SOX2*, *c-MYC* and *KLF4* exhibited similar expression changes as *OCT4*. We also assessed the expression of *NANOG,* an endogenous pluripotency factor, which was not part of the OKSM cocktail. *NANOG* was down-regulated during fibroblast de-differentiation (Figure 1D), confirming that short-term induction of 7 days did not induce pluripotency. We used Day 7 cells for subsequent studies because CD34 expression had reached a plateau and there was no evidence of pluripotency at this stage. Assessing generation of $CD34^+$ cells by flow cytometry, we found that de-differentiation of both human neonatal and adult dermal fibroblasts gave rise to $CD34^+$ cells; with higher $CD34^+$ yield from neonatal as compared to adult fibroblasts (16.3±2% vs. 8.7±1%, Figure 1E-F). We then focused on human adult dermal fibroblasts because of their potential utility for vascular regeneration in patients.

The $CD34^+$ cells were also evaluated for their clonal expansion potential and the pluripotency surface markers TRA-160 and TRA-180, endothelial surface markers VE-cadherin and CD31; and the erythroblast/erythrocyte surface marker CD235a by flow cytometry. Plating of individual $CD34^+$ cells did not result in any formation of colonies. We also found that $CD34^+$ cells did not express markers of pluripotency (Figure 1G-I), endothelial differentiation (Supplemental Figure 2A-B) or erythroblast differentiation (Supplemental Figure 2C-D),

demonstrating that the cells were undifferentiated progenitors.

**Conversion of fibroblast-derived CD34$^+$ progenitors into endothelial cells**

We isolated CD34$^+$ progenitors from the de-differentiated fibroblast population using magnetic bead sorting, and exposed the cells to an EC lineage induction medium consisting of standard endothelial growth medium supplemented with the EC differentiation factors VEGF and BMP-4 for 10 days. During the induction phase, gene expression of EC markers *VE-cadherin*, *VWF*, *CD31* and *FLK1* progressively increased (Figure 2A). The induction of CD34$^+$ cells was terminated on day 10 when EC markers levels plateaued (data not shown). Flow cytometry of cells at Day 10 demonstrated that 7.8±3% of cells were positive for VE-cadherin, 8.4±3% of cells for CD31 and 4.9±1% of cells for both surface markers (Figure 2B-C). We found 92.9±1.2% of VE-cadherin$^+$ iECs continued to express CD34 after endothelial differentiation (Supplemental Figure 2E). Western blotting established upregulation of VE-cadherin, CD31, and FLK1 in these generated cells which we termed "induced endothelial cells" (iECs) (Figure 2D). Immunocytochemistry staining demonstrated that the bulk of VE-cadherin was localized in the cytoplasm in these non-confluent iECs as opposed to the cell surface membrane where VE-cadherin is typically found in confluent adherent ECs (Figure 2E). The relatively high cytosolic VE-cadherin expression also explained why only 8% of iECs were positive for VE-cadherin by flow cytometry as it monitors the cell surface expressed protein. Since VE-cadherin trans-interactions between cells stabilize VE-cadherin at the cell membrane and promote formation of adherens junctions[20], we next co-cultured the iECs with primary adult human aortic ECs. Confocal imaging demonstrated that this increased the membrane localization of VE-cadherin such that iECs formed characteristic adherens junctions via homotypic interactions (Figure 2F). We also examined the gene expression levels of the endothelial markers *VE-cadherin*, *CD31*,

*FLK1* and *VWF* in $CD31^+$ bead-sorted iECs at day 10 of induction. The iEC mRNA levels of these endothelial markers were approximately half of those in mature human ECs, but 100-1,000 fold higher than those in fibroblasts and $CD34^+$ progenitors (Supplemental Figure 3A-D).

We next performed a transcriptomic analysis of adult fibroblasts, fibroblast-derived $CD34^+$ progenitors, iECs, and primary human ECs. A heat map of global gene expression revealed that iECs clustered with ECs, whereas $CD34^+$ progenitors clustered with fibroblasts (Figure 2G); thus, iECs exhibited gene expression profile similar to adult primary ECs whereas fibroblast-derived $CD34^+$ progenitors retained fibroblast signatures. Heat maps of EC-specific and fibroblasts-specific genes indicated that gain of EC identify and loss of fibroblast signatures occurred during the transition from $CD34^+$ cells to iECs (Figure 2H and I).

**Fibroblast derived iECs are functional endothelial cells**

Key functions of endothelial cells are to form a restrictive and dynamic barrier and upregulate cell surface adhesion molecules in response to inflammatory stimuli. Thus, we assessed trans-endothelial electrical resistance (TER) in a confluent monolayer of iECs as a measure of the barrier function. In response to thrombin, we observed a significant decrease in TER of iECs monolayers parent fibroblasts showed no such response (Figure 3A-B, and Supplemental Figure 4). Importantly, iECs exhibited restoration of the barrier, a physiologic adaptive response seen in native endothelium. We also demonstrated that iECs formed capillary networks in 2D-Matrigel (Figure 3C-D), whereas fibroblasts predominately remained as single cells or cell clusters. To evaluate responses to the pro-inflammatory cytokine TNF-α, we assessed expression of adhesion molecules VCAM1 and E-Selectin. iECs responded with upregulation of VCAM1 and E-selectin proteins (Figure 3E) and mRNA (Figure 3F) in the same manner as primary human ECs.

**Proliferation potential and telomerase expression in iECs**

As the ability of EC to proliferate is required for vascular regeneration, we assessed proliferative potential of iECs. As shown in Figure 3G-H, 20-30% of iECs were labeled with BrdU, a value similar to the proliferation rate of primary human ECs. As cell expansion induces cell senescence and results in cell cycle arrest due to continuous shortening of telomeres[21-23], we assessed whether the generated iECs represented an aging cell population. We determined telomerase activity since it maintains telomere length and protects against premature senescence in embryonic and neonatal cells[21-23]. We observed that telomerase activity of iECs, as assessed by telomeric repeat amplification protocol (TRAP), was significantly greater as compared in adult fibroblasts or primary adult human ECs (Figure 3I-J). However, despite higher telomerase activity, iECs did not show significantly elevated expression of the pluripotency transcription factor *OCT4* or the proto-oncogene *c-MYC* compared to fibroblasts (Supplemental Figure 5A-B).

**Fibroblasts give also rise erythroblasts via intermediate CD34$^+$ progenitors**

Fibroblast-derived CD34$^+$ progenitors were cultured in erythroblast induction medium for 4 days to assess the generation of erythroblasts. Unlike iECs, which remained adherent to the substrate, emerging erythroblasts detached from the CD34$^+$ cell layer. Hema 3 staining cytospin preparations of iErythroblasts showed morphology reflecting different stages of maturation from basophilic erythroblasts to polychromatic erythroblasts (Figure 4A). To address whether iErythroblasts expressed an erythroid marker, we stained the cytospin preparations for the erythroid marker glycophorin CD235a. We found that 7.1±1% of nucleated were CD235a$^+$ (Figure 4B-C). Flow cytometry demonstrated that 4.2%±0.8% of cells undergoing erythroblast induction were CD235a$^+$ (Figure 4D-E). Gene expression analysis by qPCR showed expression of human hemoglobin beta and hemoglobin gamma confirming the erythroid nature of the

generated human cells (Figure 4F). The expression levels of hematopoietic transcriptional factors – *RUNX1* and *PU.1* as well as the erythroblast transcription factor *GATA1*[24, 25] were also markedly enhanced when compared to fibroblasts (Figure 4G). Moreover, erythroid colony-forming-cell (CFC) assay demonstrated formation of distinct erythroid colonies (Figure 4H-I).

**SOX17 mediates generation of iECs from CD34$^+$ progenitors**

We next evaluated expression of vascular developmental genes during iEC induction as shown in a quantitative real-time-PCR heat map (Figure 5A). We observed that the transcriptional regulator *SOX17* (a member of Sry-transcription factor family) was significantly upregulated during iECs induction. The transcription factor *ETV2* (also known as *ER71*), which when over-expressed induced fibroblast-to-endothelial transition[11, 12] was not significantly up-regulated during lineage conversion of CD34$^+$ progenitors to iECs.

SOX17, a member of the Sry-related high mobility group domain family F (SoxF) transcriptional factors, is a key regulator of EC and hematopoietic development during embryogenesis. Thus, we next investigated whether the transcription factor SOX17 identified above was required for conversion of CD34$^+$ progenitors to iECs. *SOX17* progressively increased during the 10-day induction period (Figure 5B). Immunoblotting confirmed upregulation of SOX17 in iECs compared to fibroblasts (Figure 5C). To assess whether expression of SOX17 was required for induction of iECs, lentiviral shRNAs were used to deplete SOX17 during EC induction phase. CD34$^+$ progenitors were infected with lentiviruses encoding SOX17 shRNA or scramble shRNA on Day 1 with 95% transduction efficiency (Supplemental Figure 6A-C). Using multiple shRNA constructs, we identified a SOX17-shRNA which achieved over 90% SOX17 depletion (Supplemental Figure 6D). Depletion of SOX17 prevented the differentiation of CD34$^+$ progenitors to iECs as demonstrated by suppression of the EC specific markers (VE-cadherin,

CD31 and FLK1), both at mRNA and protein levels when compared to scrambled shRNA (Figure 5D-F).

Based on these findings, we next determined whether over-expression of SOX17 would enhance EC lineage conversion. $CD34^+$ progenitors undergoing conversion were transduced with retroviruses encoding SOX17-GFP or GFP on Day 1. We observed significant increases in mRNA and protein levels of VE-cadherin, CD31 and FLK1 when compared to controls (Figure 5G-I). Quantitative analysis with flow cytometry showed that overexpression of SOX17 enhanced EC differentiation nearly 9-fold as evidenced by increased fraction of VE-cadherin positive cells when compared to using only growth factors for EC conversion (50.9±3% vs. 6.1±2%) (Figure 5J-K). Thus, conversion of $CD34^+$ progenitors into iECs was markedly enhanced by activation of transcription factors SOX17.

**SOX17 inhibits generation of iErythroblasts from $CD34^+$ progenitors**

We next examined whether SOX17 also regulates transition of $CD34^+$ progenitors, the point of bifurcation, into iErythroblasts. Here we found the expression of SOX17 increased in $CD34^+$ progenitors when compared to the parent fibroblasts but progressively decreased during the induction of iErythroblasts (Figure 6A), consistent with the role of SOX17 in favoring EC fate conversion at the $CD34^+$ progenitor bifurcation state described above. To explore the role of SOX17 in iErythroblast generation, SOX17 was depleted using shRNA in fibroblasts before de-differentiation. Depletion of SOX17 increased the expression of the hematopoietic transcription factors *RUNX1* and *PU.1* as well as erythropoiesis-specific regulator *GATA1* during erythroblast induction (Figure 6B). Flow cytometry confirmed increased erythropoiesis upon SOX17 depletion trending towards increased erythropoiesis (Figure 6C-D). In addition, we observed that depleting SOX17 significantly increased the formation of erythroid colonies (Figure 6E-F)

consistent with the role of SOX17 in directing the fate of $CD34^+$ progenitors to either iECs or Erythroblasts; that is, presence of SOX17 favored the iEC lineage whereas its downregulation enhanced erythroid specification, indicative of the rheostat function of SOX17 at the CD34 bifurcation point.

**$CD34^+$ progenitors form blood vessels and erythrocytes *in vivo* and restore myocardial function in mice**

We next assessed the *in vivo* significance of human fibroblast-derived $CD34^+$ progenitors in giving rise to iECs and iErythroblasts. We injected growth-factor reduced Matrigel containing either $CD34^+$ progenitors, fibroblasts or primary human ECs subcutaneously into immune deficient NOD-SCID mice. Matrigel plugs explanted after 1 week showed that implantation of either primary aortic human ECs (controls) or $CD34^+$ progenitors induced formation of blood vessels whereas blood vessels did not form following implantation of fibroblasts alone (Figure 7A-C)

To evaluate whether the ECs lining the newly formed blood vessels and erythrocytes in the Matrigel plug were derived from implanted human $CD34^+$ progenitors or the host mouse vasculature, we employed a human-specific CD31 antibody to stain human vessels. We also used a human specific CD235a antibody and a mouse specific TER119 antibody to stain human and mouse erythrocytes respectively after confirming the human species-specificity (Supplemental Figure 7). Staining of explanted Matrigel plugs containing $CD34^+$ progenitors demonstrated that vessels were positive for human CD31 and had greater angiogenesis than those implanted with mature ECs (Figure 7B-C). We further found that a small fraction of erythrocytes within the vessels stained positive for human CD235a (Figure 7D). We observed that the newly formed human blood vessels predominantly contained murine erythrocytes, indicating communication

between the host mouse vasculature and newly formed vessels derived from human $CD34^+$ progenitors. Importantly, Matrigel plugs containing primary human ECs showed presence of erythrocytes derived only from host mice (Supplemental Figure 8A-B).

To further demonstrate the functionality of formed human vessels, fluorescence labeled lectins that stain species-specific endothelium were injected intravenously before harvesting Matrigel implants containing GFP labeled-$CD34^+$ progenitors or GFP labeled-fibroblasts. We used Rhodamine-labeled UEA I to assess functional human endothelium and DyLight 649-labeled GS-IB4 for mouse endothelium[26]. Co-localization of GFP and UEA $I^+$ demonstrated the functionality of $CD34^+$ progenitor derived human vessels (Figure 7E) whereas areas without GFP+/UEA $I^+$ cells predominantly consisted of GS-$IB4^+$ host mouse vessels (Figure 7E). Of note, we identified selected areas of close proximity between human $CD34^+$ progenitor cells and mouse host GS-$IB4^+$ vessels (Figure 7F and Supplemental Movie 1) which likely represented communications between the host vasculature and the neo-vessels from the implanted cells, thus explaining why systemic intravenous injection of a human-specific lectin into the mice was able to stain the $CD34^+$ progenitor derived human vessels. No UEA $I^+$ human vessels were detected in plugs implanted with fibroblasts (Figure 7G). We also found examples of $GFP^+$ erythrocytes (Supplemental Figure 9), further confirming the capacity of $CD34^+$ progenitors to mature into erythrocytes *in vivo*.

To assess the teratoma-forming capacity of $CD34^+$ progenitors, NOD-SCID mice were implanted with $CD34^+$ progenitors or iPSCs (positive control) and observed for 8 weeks. We found that the implantation of iPSCs for 8 weeks formed teratomas whereas the $CD34^+$ progenitors did not form any teratomas, thus underscoring their safety and lack of pluripotency (Supplemental Figure 10A-D).

We next used a mouse myocardial infarction (MI) model to assess whether $CD34^+$ progenitors enhance perfusion and cardiac function. We injected a Matrigel suspension containing either $CD34^+$ progenitors or control fibroblasts in the peri-infarct area following left coronary artery ligation. Masson trichrome staining of cross section of hearts on Day 14 post-MI showed reduced fibrosis in hearts injected with $CD34^+$ progenitors (Figure 8A). Heart weight/body weight ratio was also decreased in mice receiving $CD34^+$ progenitors (Figure 8B), indicating suppression of adverse remodeling after infarction. Echocardiography demonstrated significantly improved cardiac contractility, as measured by ejection fraction (Figure 8C) and fractional shortening (Figure 8D) at 1 and 2 weeks post-MI in hearts receiving $CD34^+$ progenitors when compared to hearts which received control fibroblasts. $CD34^+$ progenitor implantation also improved morphologic and hemodynamic indices as assessed by echocardiography (Supplemental Table 1). $CD34^+$ cells were transduced with GFP prior to transplantation to track the fate of implanted cells. Immunofluorescence demonstrated that the implantation of $CD34^+$ progenitors resulted in formation of human $CD31^+$ blood vessels while implantation of human fibroblasts formed none (Supplemental Figure 11A-C). We also observed that human $CD31^+$ blood vessels were integrated with host mouse $CD31^+$ vasculature (Supplemental Figure 11B and Supplemental Movie 2).

To further confirm the functionality of human neo-vessels in the myocardium, fluorescence-labeled UEA I and GS-IB4 were intravenously injected before harvesting the heart. We observed that GFP co-localized with UEA I (Figure 8E-F), demonstrating that implantation of $CD34^+$ progenitors formed functional human vessels in the myocardium after myocardial infarction.

## Discussion

Here we demonstrate a novel approach for re-programming of human fibroblasts into ECs that also gives rise to erythroblasts via the de-differentiation into intermediate $CD34^+$ progenitors. We identified the developmental transcription factor SOX17 as a tunable rheostat like switch converting $CD34^+$ cells to both lineages. Implantation of human $CD34^+$ progenitors in NOD/SCID mice gave rise to human ECs capable of forming blood vessels carrying erythrocytes, markedly enhancing human microvessel generation and cardiac function after myocardial infarction. Unlike pluripotent stem cells, fibroblasts de-differentiated to $CD34^+$ progenitors did not form any teratomas following implantation, thus underscoring their safety for translational applications in vascular engineering and revascularization. Importantly, systemic intravenous injections of human and mouse lectins into the recipient mice demonstrate that the neo-vessels formed by the implanted human fibroblast-derived $CD34^+$ progenitor cells are functional and communicate with the host mouse vasculature.

Previous approaches to generating ECs from fibroblasts involved the ectopic expression of EC specific transcription factors[11, 12], which have relatively low yield and persistence of fibroblast markers, thus limiting their therapeutic potential. Other approaches involved de-differentiation via Yamanaka factors without genetically directing cells towards the EC lineage[8-10]. In the present study, we show a third strategy involving the generation of intermediate de-differentiated $CD34^+$ progenitors and then genetically modulating the transcription factor SOX17 to direct lineage fate to iECs and iErythroblasts. Thus, in this method the intermediate $CD34^+$ progenitors can be directed to form both iECs and erythroid lineage cells with therapeutic potential. After purification for $CD34^+$ cells using magnetic beads, not all cells expressed $CD34^+$ by subsequent flow cytometric analysis which may be indicative of CD34 internalization or

differences in the specificity and sensitivity between magnetic bead sorting and flow cytometry analysis.

To define transcriptional mechanisms underlying the generation of iECs and erythrocytes we identified by transcriptomic analysis of $CD34^+$ cells the requisite role of SOX17 as an essential transcription factor responsible for the conversion. SOX17, a member of the Sry-related high mobility group domain family F(SoxF) transcriptional factor[27], is a key regulator of endothelial and hematopoietic developmental during embryogenesis[28-32]. We showed that SOX17 was required for endothelial lineage conversion and that its over-expression markedly enhanced the generation of iECs from fibroblasts. Further, depletion of SOX17 facilitated the generation of erythrocytes. The regulatory role of SOX17 at the CD34 bifurcation point specified the conversion to iEC and iErythroblast fates. This is reminiscent of the role of SOX17 during embryonic development during which SOX17 regulates EC to hematopoietic fate switch[33]; specifically loss of SOX17-mediated repression of hematopoietic transcription factors Runx1 and Gata2 prevented EC generation and augmented blood cell generation[33].

The described method of iEC and iErythroblast generation has a distinct advantage in that it describes for the first time the generation of cells capable of forming blood vessels and also erythrocytes *in vivo*. We demonstrated that transplantation of $CD34^+$ progenitors in subcutaneous Matrigel plugs induced formation of blood vessels comprised of human ECs and perfused with human erythrocytes. A likely mechanism by which transplanted $CD34^+$ progenitors give rise to both cells may be the release of endothelial differentiation cues in ischemic niche such as VEGF and the presence of erythropoietin in the circulating blood[34-37] which in turn fine tune SOX17 expression to optimize generation of both cells.

Our transcriptomic analysis of $CD34^+$ progenitors and iECs indicated that iECs

exhibited the gene expression profile similar to adult primary ECs whereas $CD34^+$ progenitors retained fibroblast signatures such as collagen1a and collagen3a. Gain of EC identify and concomitant loss of fibroblast identity occurred during the transition from $CD34^+$ progenitor state to the iEC state. Although $CD34^+$ progenitors exhibited residual fibroblast gene expression, implantation of $CD34^+$ progenitors in the infarcted myocardium reduced fibrosis, suggesting that the imprinted fibroblast "memory" was lost in situ in the ischemic environment.

Previous studies described the role of ETV2 (ER71) in inducing fibroblast to endothelial conversion[11, 12]; however, we did not find its significant upregulation. Our approach was guided by unbiased transcriptomic analysis of endogenous transcription factors upregulated during de-differentiation and lineage conversion. Although endogenous ETV2 was not upregulated during de-differentiation its over-expression can direct fibroblasts towards EC lineage[11, 12]. Our results are in accord with an interesting lineage tracing study showing that p53 signaling mediated in situ conversion of endogenous fibroblasts to ECs lead to improved cardiac function after myocardial infarction[38], although these studies did not address whether there was an intermediate $CD34^+$ progenitor cell responsible for EC conversion. Recent studies also shown that innate immunity is a critical regulator for reprogramming of fibroblasts into the pluripotent state as well as transdifferentiating fibroblasts to ECs[39, 40]. Since myocardial infarction activates inflammatory pathways and innate immunity, it is possible that this serves as a cue for implanted $CD34^+$ cells to initiate in situ reprogramming to iECs and iErythroblasts.

SOX17 together with Notch1 regulates the embryonic EC-hematopoietic fate transition [33, 41]. SOX17 prevented hematopoietic cell fate of hemangioblasts and hemogenic ECs by repressing the expression of hematopoietic transcription factors whereas loss of SOX17 instructed differentiation towards hematopoietic fate[33]. We did not examine the role of Notch1 in

regulating $CD34^+$ cell to iEC transition because our transcriptomic analysis showed that it did not increase during transdifferentiation. In addition, SOX17 was selectively expressed in mouse embryonic and adult arterial ECs where it was required for maintaining arterial identity[42] and integrity[43] consistent with our finding of the essential importance of SOX17 in mediating generation of iECs. It has also been recently shown that SOX17 expression can enhance the maturation and engraftment of endothelial cells derived from amniotic cells[44]. It is therefore possible that the SOX17 expression in fibroblast-derived ECs similarly helped mature and engraft the ECs derived from the progenitors we implanted.

In addition to identifying the bi-lineage differentiation potential of fibroblast derived $CD34^+$ progenitors and obligatory role of SOX17 in iEC and iErythroblast generation, we found that de-differentiation upregulated telomerase activity of iECs. This may be the result of the initial introduction of pluripotency factors that activated embryonic transcriptional programs. Activation of telomerase may be important for autologous cell therapy which requires extensive *in vitro* cell expansion because telomeres undergo shortening during cell expansion[21-23]. We found that de-differentiation in fact upregulated telomerase in the $CD34^+$ progenitors undergoing lineage conversion, which may induce generation of blood vessels with greater survival advantage in ischemic tissue. Interestingly, the de-differentiation of adult ECs to vascular progenitors has also been shown the generate cells with significant vascularization potential[45] which may also reflect some resilience to senescence.

We cannot exclude the possibility that the $CD34^+$ progenitor cells derived from fibroblasts contain subpopulations of cells which may be poised to give rise only to endothelial or erythroid lineage cells. However, our flow cytometric analysis of the $CD34^+$ population did not show any evidence of endothelial or erythroid markers, suggesting that they are uncommitted

at this stage.

In summary, our studies establish a novel role for the transcription factor - SOX17 as a critical endogenous regulator of the transition from fibroblasts to ECs and erythrocytes via the de-differentiation to $CD34^+$ progenitors (Figure 8G). De-differentiation of adult fibroblasts in part recapitulates embryonic development as evidenced by the generation of progenitors which can give rise to endothelial and erythroid cells and express telomerase. $CD34^+$ progenitors *in situ* gave rise to functional human ECs and erythrocytes and displayed profound vasculogenesis and restored cardiac function post-transplantation, thus highlighting the potential therapeutic role of such progenitors.



**Acknowledgements**

L.Z., A.J., Z.H., S.K., G.M., Y.Y., P.T. and B.H. performed the experiments. L.Z, A.B.M. and J.R. designed the experiments. L.Z., A.J., B.H. and J.R. analyzed and interpreted the data. L.Z., A.B.M and J.R. wrote the manuscript. We would like to thank Jillian Koziel for her assistance in performing the telomerase activity assays and Yang Yuan for her assistance in histological analysis.

**Sources of Funding**

This work was supported in part by the National Institutes of Health: R01GM094220, R01HL118068, T32HL007829 and R01HL090152.

**Disclosures**

None

## References

1. Zhang L, Malik AB and Rehman J. Reprogramming fibroblasts to endothelial cells: converted or born again? Circulation. 2014;130:1136-1138.
2. Capellera-Garcia S, Pulecio J, Dhulipala K, Siva K, Rayon-Estrada V, Singbrant S, Sommarin MN, Walkley CR, Soneji S, Karlsson G, Raya A, Sankaran VG and Flygare J. Defining the Minimal Factors Required for Erythropoiesis through Direct Lineage Conversion. Cell Rep. 2016;15:2550-2562.
3. Efe JA, Hilcove S, Kim J, Zhou H, Ouyang K, Wang G, Chen J and Ding S. Conversion of mouse fibroblasts into cardiomyocytes using a direct reprogramming strategy. Nat Cell Biol. 2011;13:215-222.
4. Huang P, He Z, Ji S, Sun H, Xiang D, Liu C, Hu Y, Wang X and Hui L. Induction of functional hepatocyte-like cells from mouse fibroblasts by defined factors. Nature. 2011;475:386-389.
5. Ieda M, Fu JD, Delgado-Olguin P, Vedantham V, Hayashi Y, Bruneau BG and Srivastava D. Direct reprogramming of fibroblasts into functional cardiomyocytes by defined factors. Cell. 2010;142:375-386.
6. Vierbuchen T, Ostermeier A, Pang ZP, Kokubu Y, Sudhof TC and Wernig M. Direct conversion of fibroblasts to functional neurons by defined factors. Nature. 2010;463:1035-41.
7. Panopoulos AD, Ruiz S and Izpisua Belmonte JC. iPSCs: induced back to controversy. Cell Stem Cell. 2011;8:347-348.
8. Kurian L, Sancho-Martinez I, Nivet E, Aguirre A, Moon K, Pendaries C, Volle-Challier C, Bono F, Herbert JM, Pulecio J, Xia Y, Li M, Montserrat N, Ruiz S, Dubova I, Rodriguez C, Denli AM, Boscolo FS, Thiagarajan RD, Gage FH, Loring JF, Laurent LC and Izpisua Belmonte JC. Conversion of human fibroblasts to angioblast-like progenitor cells. Nat Methods. 2013;10:77-83.
9. Li J, Huang NF, Zou J, Laurent TJ, Lee JC, Okogbaa J, Cooke JP and Ding S. Conversion of human fibroblasts to functional endothelial cells by defined factors. Arterioscler Thromb Vasc Biol. 2013;33:1366-1375.
10. Margariti A, Winkler B, Karamariti E, Zampetaki A, Tsai TN, Baban D, Ragoussis J, Huang Y, Han JD, Zeng L, Hu Y and Xu Q. Direct reprogramming of fibroblasts into endothelial cells capable of angiogenesis and reendothelialization in tissue-engineered vessels. Proc Natl Acad Sci U S A. 2012;109:13793-13798.
11. Han JK, Chang SH, Cho HJ, Choi SB, Ahn HS, Lee J, Jeong H, Youn SW, Lee HJ, Kwon YW, Cho HJ, Oh BH, Oettgen P, Park YB and Kim HS. Direct conversion of adult skin fibroblasts to endothelial cells by defined factors. Circulation. 2014;130:1168-1178.
12. Morita R, Suzuki M, Kasahara H, Shimizu N, Shichita T, Sekiya T, Kimura A, Sasaki K, Yasukawa H and Yoshimura A. ETS transcription factor ETV2 directly converts human fibroblasts into functional endothelial cells. Proc Natl Acad Sci U S A. 2015;112:160-165.
13. Hirschi KK. Hemogenic endothelium during development and beyond. Blood. 2012;119:4823-4827.
14. Lancrin C, Sroczynska P, Stephenson C, Allen T, Kouskoff V and Lacaud G. The haemangioblast generates haematopoietic cells through a haemogenic endothelium stage. Nature. 2009;457:892-895.
15. Palis J, Robertson S, Kennedy M, Wall C and Keller G. Development of erythroid and myeloid progenitors in the yolk sac and embryo proper of the mouse. Development.

1999;126:5073-5084.
16. Lu SJ, Feng Q, Caballero S, Chen Y, Moore MA, Grant MB and Lanza R. Generation of functional hemangioblasts from human embryonic stem cells. Nat Methods. 2007;4:501-509.
17. Peters A, Burridge PW, Pryzhkova MV, Levine MA, Park TS, Roxbury C, Yuan X, Peault B and Zambidis ET. Challenges and strategies for generating therapeutic patient-specific hemangioblasts and hematopoietic stem cells from human pluripotent stem cells. Int J Dev Biol. 2010;54:965-990.
18. Sidney LE, Branch MJ, Dunphy SE, Dua HS and Hopkinson A. Concise review: evidence for CD34 as a common marker for diverse progenitors. Stem Cells. 2014;32:1380-1389.
19. Paul JD, Coulombe KL, Toth PT, Zhang Y, Marsboom G, Bindokas VP, Smith DW, Murry CE and Rehman J. SLIT3-ROBO4 activation promotes vascular network formation in human engineered tissue and angiogenesis in vivo. J Mol Cell Cardiol. 2013;64:124-131.
20. Daneshjou N, Sieracki N, van Nieuw Amerongen GP, Schwartz MA, Komarova YA, Malik AB and Conway DE. Rac1 functions as a reversible tension modulator to stabilize VE-cadherin trans-interaction. J Cell Biol. 2015;208:23-32.
21. Armanios M. Telomeres and age-related disease: how telomere biology informs clinical paradigms. J Clin Invest. 2013;123:996-1002.
22. Blasco MA. Telomere length, stem cells and aging. Nat Chem Biol. 2007;3:640-9.
23. Rando TA and Chang HY. Aging, rejuvenation, and epigenetic reprogramming: resetting the aging clock. Cell. 2012;148:46-57.
24. Takeuchi M, Fuse Y, Watanabe M, Andrea CS, Takeuchi M, Nakajima H, Ohashi K, Kaneko H, Kobayashi-Osaki M, Yamamoto M and Kobayashi M. LSD1/KDM1A promotes hematopoietic commitment of hemangioblasts through downregulation of Etv2. Proc Natl Acad Sci U S A. 2015;112:13922-13927.
25. Hewitt KJ, Sanalkumar R, Johnson KD, Keles S and Bresnick EH. Epigenetic and genetic mechanisms in red cell biology. Curr Opin Hematol. 2014;21:155-164.
26. Kang KT, Allen P and Bischoff J. Bioengineered human vascular networks transplanted into secondary mice reconnect with the host vasculature and re-establish perfusion. Blood. 2011;118:6718-6721.
27. Park C, Kim TM and Malik AB. Transcriptional regulation of endothelial cell and vascular development. Circ Res. 2013;112:1380-1400.
28. Choi KD, Vodyanik MA, Togarrati PP, Suknuntha K, Kumar A, Samarjeet F, Probasco MD, Tian S, Stewart R, Thomson JA and Slukvin, II. Identification of the hemogenic endothelial progenitor and its direct precursor in human pluripotent stem cell differentiation cultures. Cell Rep. 2012;2:553-567.
29. Clarke RL, Yzaguirre AD, Yashiro-Ohtani Y, Bondue A, Blanpain C, Pear WS, Speck NA and Keller G. The expression of Sox17 identifies and regulates haemogenic endothelium. Nat Cell Biol. 2013;15:502-510.
30. Lee SH, Lee S, Yang H, Song S, Kim K, Saunders TL, Yoon JK, Koh GY and Kim I. Notch pathway targets proangiogenic regulator Sox17 to restrict angiogenesis. Circ Res. 2014;115:215-226.
31. Nakajima-Takagi Y, Osawa M, Oshima M, Takagi H, Miyagi S, Endoh M, Endo TA, Takayama N, Eto K, Toyoda T, Koseki H, Nakauchi H and Iwama A. Role of SOX17 in hematopoietic development from human embryonic stem cells. Blood. 2013;121:447-458.
32. Niakan KK, Ji H, Maehr R, Vokes SA, Rodolfa KT, Sherwood RI, Yamaki M, Dimos JT,

Chen AE, Melton DA, McMahon AP and Eggan K. Sox17 promotes differentiation in mouse embryonic stem cells by directly regulating extraembryonic gene expression and indirectly antagonizing self-renewal. Genes Dev. 2010;24:312-326.
33. Lizama CO, Hawkins JS, Schmitt CE, Bos FL, Zape JP, Cautivo KM, Borges Pinto H, Rhyner AM, Yu H, Donohoe ME, Wythe JD and Zovein AC. Repression of arterial genes in hemogenic endothelium is sufficient for haematopoietic fate acquisition. Nat Commun. 2015;6:7739-7748.
34. Arany Z, Foo SY, Ma Y, Ruas JL, Bommi-Reddy A, Girnun G, Cooper M, Laznik D, Chinsomboon J, Rangwala SM, Baek KH, Rosenzweig A and Spiegelman BM. HIF-independent regulation of VEGF and angiogenesis by the transcriptional coactivator PGC-1alpha. Nature. 2008;451:1008-1012.
35. Lemus-Varela ML, Flores-Soto ME, Cervantes-Munguia R, Torres-Mendoza BM, Gudino-Cabrera G, Chaparro-Huerta V, Ortuno-Sahagun D and Beas-Zarate C. Expression of HIF-1 alpha, VEGF and EPO in peripheral blood from patients with two cardiac abnormalities associated with hypoxia. Clin Biochem. 2010;43:234-239.
36. Rankin EB, Biju MP, Liu Q, Unger TL, Rha J, Johnson RS, Simon MC, Keith B and Haase VH. Hypoxia-inducible factor-2 (HIF-2) regulates hepatic erythropoietin in vivo. J Clin Invest. 2007;117:1068-1077.
37. Semenza GL, Nejfelt MK, Chi SM and Antonarakis SE. Hypoxia-inducible nuclear factors bind to an enhancer element located 3' to the human erythropoietin gene. Proc Natl Acad Sci U S A. 1991;88:5680-5684.
38. Ubil E, Duan J, Pillai IC, Rosa-Garrido M, Wu Y, Bargiacchi F, Lu Y, Stanbouly S, Huang J, Rojas M, Vondriska TM, Stefani E and Deb A. Mesenchymal-endothelial transition contributes to cardiac neovascularization. Nature. 2014;514:585-590.
39. Lee J, Sayed N, Hunter A, Au KF, Wong WH, Mocarski ES, Pera RR, Yakubov E and Cooke JP. Activation of innate immunity is required for efficient nuclear reprogramming. Cell. 2012;151:547-558.
40. Sayed N, Wong WT, Ospino F, Meng S, Lee J, Jha A, Dexheimer P, Aronow BJ and Cooke JP. Transdifferentiation of human fibroblasts to endothelial cells: role of innate immunity. Circulation. 2015;131:300-309.
41. Gama-Norton L, Ferrando E, Ruiz-Herguido C, Liu Z, Guiu J, Islam AB, Lee SU, Yan M, Guidos CJ, Lopez-Bigas N, Maeda T, Espinosa L, Kopan R and Bigas A. Notch signal strength controls cell fate in the haemogenic endothelium. Nat Commun. 2015;6:8510-8521.
42. Corada M, Orsenigo F, Morini MF, Pitulescu ME, Bhat G, Nyqvist D, Breviario F, Conti V, Briot A, Iruela-Arispe ML, Adams RH and Dejana E. Sox17 is indispensable for acquisition and maintenance of arterial identity. Nat Commun. 2013;4:2609-2612.
43. Lee S, Kim IK, Ahn JS, Woo DC, Kim ST, Song S, Koh GY, Kim HS, Jeon BH and Kim I. Deficiency of endothelium-specific transcription factor sox17 induces intracranial aneurysm. Circulation. 2015;131:995-1005.
44. Schachterle W, Badwe CR, Palikuqi B, Kunar B, Ginsberg M, Lis R, Yokoyama M, Elemento O, Scandura JM and Rafii S. Sox17 drives functional engraftment of endothelium converted from non-vascular cells. Nat Commun. 2017;8:13963-13974.
45. Yin L, Ohanyan V, Pung YF, Delucia A, Bailey E, Enrick M, Stevanov K, Kolz CL, Guarini G and Chilian WM. Induction of vascular progenitor cells from endothelial cells stimulates coronary collateral growth. Circ Res. 2012;110:241-252.

## Figure Legends

**Figure 1. Generating CD34$^+$ progenitors from human dermal fibroblasts. (A)** Schematic of converting human dermal fibroblasts into induced endothelial cells (iECs) and induced Erythroblasts (iErythroblasts) via sorted CD34$^+$ progenitors from de-differentiated fibroblasts (De-Diff-Fib) at day 7. **(B-D)** Quantitative PCR analysis of the mesodermal marker *CD34* (**B**), and pluripotency markers *OCT4* (**C**) and *Nanog* (**D**) during adult fibroblast de-differentiation from day 0 to day 7; n=4. **(E)** Representative flow cytometry plots of the mesodermal marker CD34$^+$ in fibroblasts, adult De-Diff-Fib, and neonatal De-Diff-Fib. **(F)** Quantification and statistical analysis of CD34$^+$ cells in fibroblasts (n=3), Adult De-Diff-Fib (n=6) and Neonatal De-Diff-Fib (n=6) from flow cytometry. **(G-I)** Representative flow cytometry overlay plots of the pluripotency markers – human TRA-160 and TRA-180 in CD34$^+$ progenitors (**G**) and iPSCs (**H**), and quantification of TRA-160 or TRA-180 positive cells (**I**) in CD34$^+$ progenitors and iPSCs. Data are presented as mean ± SE, *P<0.05, **P<0.01, ***P<0.001, compared to Day 0 in **B**, **C**, and **D**, compared to fibroblasts in **F**, using repeated measures one-way ANOVA in **B**, **C**, **D**, and one-way ANOVA in **F**. N.D., not detected in **I**.

**Figure 2. Induction of endothelial cells**. **(A)** Quantitative PCR analysis of endothelial specific genes - *VE-cadherin*, *CD31*, *VWF*, and *FLK1* in iECs from day 0 to day 10, normalized to day 0, n=3. **(B)** Representative flow cytometry plots of endothelial markers - VE-cadherin and CD31 at day 10 in human aortic endothelial cells (ECs) and iECs. **(C)** Quantification of VE-cadherin$^+$ and CD31$^+$ cells in iECs at day 10 from flow cytometry, n=4. **(D)** Immunoblots of the endothelial specific proteins – human VE-cadherin, CD31and FLK1 in iECs and fibroblasts, beta-Actin

served as a control. **(E)** Representative micrographs of immunocytochemistry staining of human VE-cadherin (green) and human CD31 (red) of iECs at day 10, nuclei were stained by DAPI. Scale bars: 50μm. **(F)** Confocal micrographs of immunofluorescence staining of human VE-cadherin (red) after cocultured iECs (labeled by CytoTracker Green) and ECs (labeled by CytoTracker Far Red, pseudo colored as orange) for 2 days. Scale bars: 20μm. **(G-I)** Analysis of cDNA microarrays in adult fibroblasts, $CD34^+$ progenitors (labeled as $CD34^+$ ), iECs, and ECs - heat map of global gene using hierarchical clustering analysis (**G**), heat map of endothelial genes (**H**) and fibroblast genes (**I**). The color bars indicate gene expression level in $\log_2$ scale. Blue to red color represents low to high expression level. Data are presented as mean ± SE; *P<0.05, **P<0.01, ***P<0.001, compared to day 0. $^{\#}$P<0.05, $^{\#\#}$P<0.01, $^{\#\#\#}$P<0.001, compared to day 3; $^{\&}$P<0.05, $^{\&\&\&}$P<0.05 compared to day 7 using repeated measures one-way ANOVA in **A**.

**Figure 3. Characterization of iECs.** **(A-B)** The permeability of iECs in response to thrombin. Trans-endothelial electrical resistance (TER) was measured for 90 minutes in fibroblasts and iECs. Thrombin (3.5μg/ml;0.5 unit) was added as indicated. The time course of resistance in fibroblasts and iECs normalized to baseline (**A**) and statistical analysis of percentage of deduction of resistance in response to thrombin in fibroblasts and iECs, n=4 (**B**). **(C-D)** In vitro capillary network formation of iECs and fibroblasts on Matrigel. The representative images (**C**) and statistical analysis (**D**) of tube network formation in fibroblasts, iECs and ECs, n=3. **(E-F)** The inflammation response of iECs. FACS analysis (**E**) and quantitative realtime-PCR measurement (**F**) for CD106 and CD62E on TNF-α activated ECs and iECs, n=3. **(G-H)** The proliferation of iECs. Representative flow cytometry plots (**G**) of the proliferation capacity of iECs and ECs as assessed by BrdU uptake and statistical analysis (**H**) of the percentage of $BrdU^+$

cells in iECs and ECs, n=3. **(I-J)** The telomerase activity of iECs. Telomerase activity was measured by a telomeric repeat amplification protocol (TRAP) assay. PCR amplification results of TRAP (**I**) from positive control, negative control, fibroblasts, ECs and iECs and statistical analysis (**J**) of telomerase activity in above cell types, n=3. Data are presented as mean ± SE; *P<0.05, **P<0.01, ***P<0.001, N.S. P>0.05; compared to fibroblasts in **B**, **D**, **E**, **F**, and **J**; compared to ECs in **E**, **F** and **H**, using Student's t-test in **B** and **H**, one-way ANOVA in **J** and two-way ANOVA in **E** and **F.**



**Figure 4. Induction and characterization of iErythroblasts.** **(A)** The representative Hema 3 staining images of iErythroblasts. Scale bars: 20μm. **(B-C)** The immunocytochemistry analysis of erythrocyte markers CD235a in iErythroblasts - the representative immunofluorescence images of iErythroblasts (**B**) and statistical analysis of percentage of $CD235a^+$ cells in fibroblasts and iErythroblasts (**C**). Scale bars: 20μm. n=4. **(D-E)** FACS analysis of erythrocyte markers CD235a. The representative flow cytometry plots (**D**) and statistical analysis (**E**) of percentage of $CD235a^+$ cells in iErythroblasts and fibroblasts, n=6. **(F)** Quantitative PCR analysis of hemoglobin β and hemoglobin γ by Taqman assay in the fibroblasts and iErythroblasts, n=3. **(G)** Quantitative PCR analysis of transcriptional factors of hematopoietic cells – *GATA1*, *RUNX1* and *PU.1* in fibroblasts and iErythroblasts, n=4. **(H-I)** Erythroid Colony- Forming-Cell (CFC) assays. Representative erythroid colony images (**H**) and statistical analysis (**I**) of erythroid colony numbers of fibroblasts and iErythroblasts, n= 3. Data are presented as mean ± SE; *P<0.05, **P<0.01, ***P<0.001, compared to fibroblasts, using Student's *t* test in **C**, **E,** and **I** and Student's t test with multiple comparisons (Bonferroni Correction) in **F** and **G**.

**Figure 5. SOX17 is required for the induction of iECs from CD34$^+$ progenitors. (A)** Heat map of endothelial developmental genes during iEC induction (iECs at day 0, day 3, day 7 and day 10) by quantitative realtime-PCR. The color key indicates gene expression level relative to $B_2M$ normalized to iECs at day 0. Blue to red color represents low to high expression level. **(B-C)** The expression level of *SOX17* in iECs. The time course of mRNA level of *SOX17* during the induction of iECs, n=4, (**B**). Immunoblot of SOX17 in adult fibroblasts and iECs (**C**). **(D-F)** The representative immunoblots (**D**) and their statistical analysis (**E**), and the quantitative PCR analysis (**F**) of SOX17, and EC specific markers – VE-cadherin, CD31 and FLK1 in iECs infected with lentivirus expressing SOX17 shRNA or scramble shRNA, n=4. **(G-I)** The representative immunoblots (**G**) and their statistical analysis (**H**), and the quantitative PCR analysis (**I**) of SOX17, and EC specific markers – VE-cadherin, CD31 and FLK1 in iECs infected with retrovirus expressing SOX17-GFP or GFP, n=4. **(J-K)** Representative flow cytometry overlay plots of the endothelial markers - VE-cadherin (**J**) and statistical analysis of percentage of VE-cadherin positive cells (**K**) in iECs overexpressed with SOX17-GFP or GFP. Data are presented as mean ± SE. *P<0.05, ***P<0.001, compared to day 0 in **A**; $^{\#}$P<0.05, $^{\#\#\#}$P<0.001, compared to day 3 in **A**; $^{\&}$P<0.05 compared to day 7 in **A**. *P<0.05, **P<0.01, compared to control in **E**, **F, H** and **I**. Using repeated measures one-way ANOVA in **B**, Student's t test with multiple comparisons (Bonferroni Correction) in **E**, **F**, **H** and **I** and Student's t test in **K**.

**Figure 6. Depletion of SOX 17 facilitates the induction of erythroblasts from CD34$^+$ progenitors. (A)** Quantitative PCR analysis of *SOX17* in fibroblasts, CD34$^+$ progenitors, and iErythroblasts at day 2 and 4, n=3. **(B)** The gene expression levels of hematopoietic transcription

factors (*GATA1*, *PU.1*, *RUNX*) and *SOX17* in iErythroblasts infected with lentivirus expressing SOX17-1shRNA using scramble shRNA as control. **(C-D)** Representative flow cytometry overlay plots of the erythroblasts/erythrocytes markers – human CD235a (**C**) and statistical analysis of percentage of $CD235a^+$ cells in iErythroblasts infected with lentivirus expressing SOX17 shRNA or scramble shRNA (**D**). **(E-F)** The representative images (**E**) and statistical analysis (**F**) of Erythroid Colony- Forming-Cell (CFC) assays in iErythroblasts infected with SOX17 shRNA or scramble shRNA. The infected cells expressed GFP because the pLL3.7-GFP lentivectors were applied to express SOX17 shRNA or scramble shRNA. Data are presented as mean ± SE, *P<0.05, **P<0.01, compared to fibroblasts in **A**, compared to scramble shRNA in **B**, **D** and **F**, using one-way ANOVA in **A**, Student's t test with multiple comparisons (Bonferroni Correction) in **B** and Student's t test in **D** and **F**.



**Figure 7. *In vivo* angiogenesis of fibroblast derived $CD34^+$ progenitors. (A)** Representative gross images (top) and H&E staining images of section (bottom) of explanted gels at day 7 of the angiogenesis assay. (**B-D**) Representative confocal micrographs (**B)** of immunohistochemistry staining of human CD235a (red, left) or mouse TER119 (red, right) and anti- human CD31 (green) in the explanted plugs of $CD34^+$ progenitors. Nuclei stained by DAPI. Scale bars, 5μm. (**C-D**) The quantification and statistical analysis of human vessels ($CD31^+$) in the explanted plugs of $CD34^+$ progenitors, ECs or fibroblasts (**C**), and the composition of vessels ($CD31^+$) with human RBC ($CD235a^+$) in the explanted plugs of $CD34^+$ progenitors, and ECs (**D**), N.D., not detected. (**E-G**) The analysis of functionality of human vessels formed by GFP-labeled $CD34^+$ progenitors in the angiogenesis plugs. UEA I (labels human endothelium) and GS-IB4 (labels mouse endothelium) were intravenously injected one hour before explantation of plugs.

Representative confocal images of human vessels (red) and mouse host vessels (magenta) (**E**), and integration of human vessels (red) and mouse host vessels (magenta) in the plugs implanted with human $CD34^+$ progenitors (**F**). The quantification of UEA $I^+$ vessels in the plugs implanted with $CD34^+$ progenitors and ECs **(G)**. Data are presented as mean ± SE. *P<0.05, ***P<0.001, compared to fibroblasts in **C**, compared to ECs in **C**, **D** and **G**, using one-way ANOVA in **C** and Student's t test in **D** and **G**.

**Figure 8. Regenerative potential of fibroblast derived $CD34^+$ progenitors following myocardial infarction (A)** Images of Masson's trichrome staining of myocardial cross-sections at 2 weeks post MI and M-mode echocardiography images at baseline, 1 week post MI and 2 weeks post MI. **(B-D)** The statistical analysis of heart weight/ body weight (**B**) at 2 weeks post MI with $CD34^+$ progenitor or fibroblast treatment, ejection fraction (**C**) and fraction shortening (**D**) at baseline (before MI), 1 week post MI, and 2 weeks post MI with $CD34^+$ progenitor or fibroblast treatment. **(E)** UEA I and GS-IB4 (intravenously injected one hour before heart explantation). Representative confocal micrographs of myocardial cross-section at 2 week post MI implanted with GFP pre-labeled human $CD34^+$ progenitor treatment. Nuclei stained with DAPI (blue). Scale bars, 50μm. **(F)** Human vessels (UEA $I^+$, red) were quantified per $40mm^2$ visual field in sections of the heart that were in proximity to the injection sites at 2 weeks post-MI with human $CD34^+$ progenitor (n=6) or fibroblast (n=4) treatment, N.D., not detected. Data are presented as mean ± SE. *P<0.05, **P<0.01, ***P<0.001, compared to fibroblasts using Student's t-test in **B** and **F**; and repeated measures two-way ANOVA in **C** and **D**. **(G)** Overview of a differential role of SOX17 in the induction of endothelial cells and erythroblasts from $CD34^+$ progenitors.

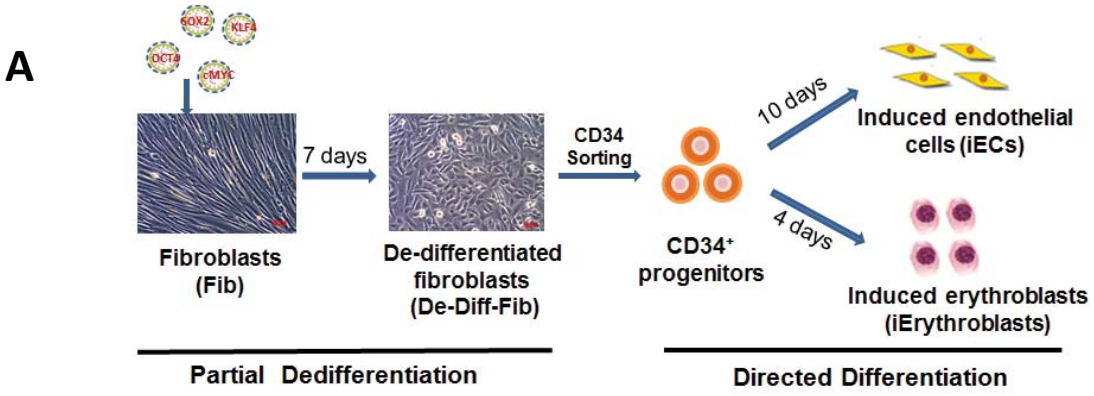


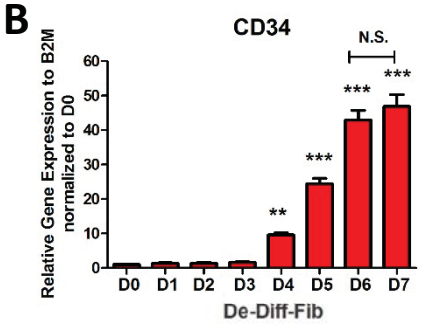


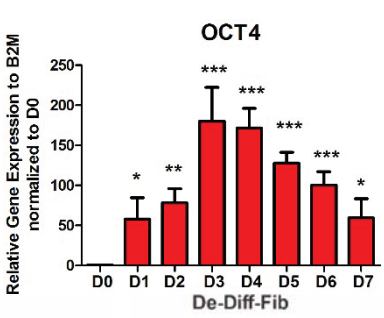


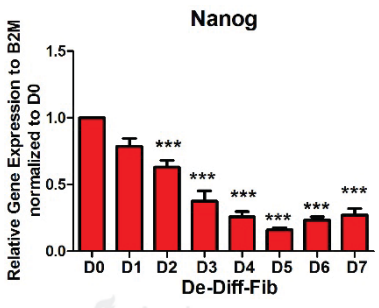


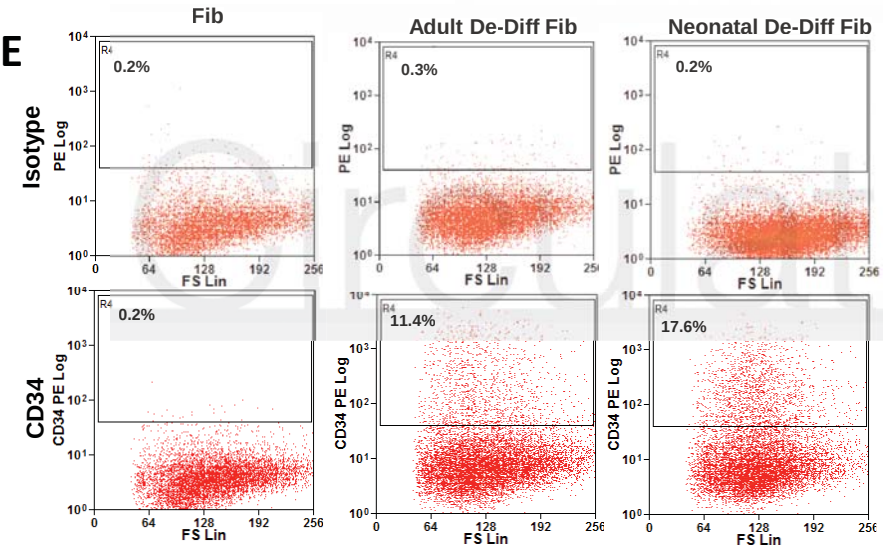


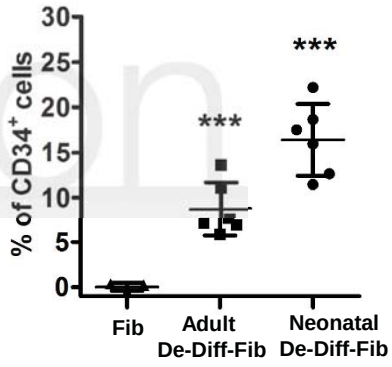


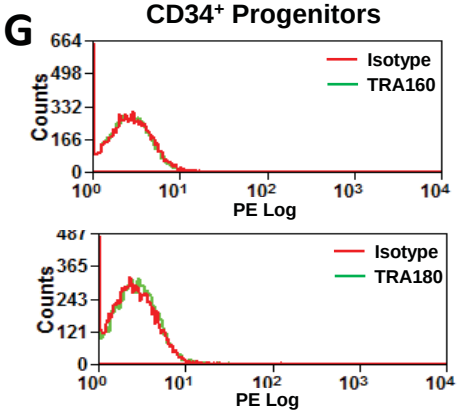


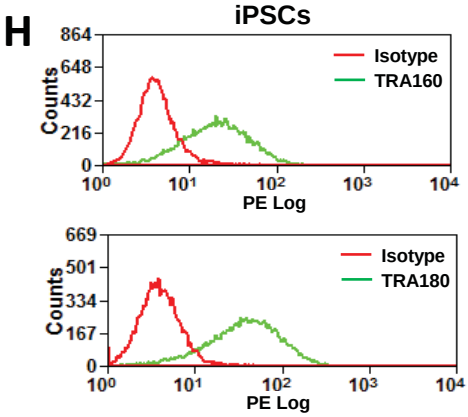


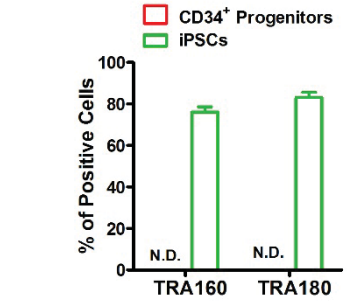

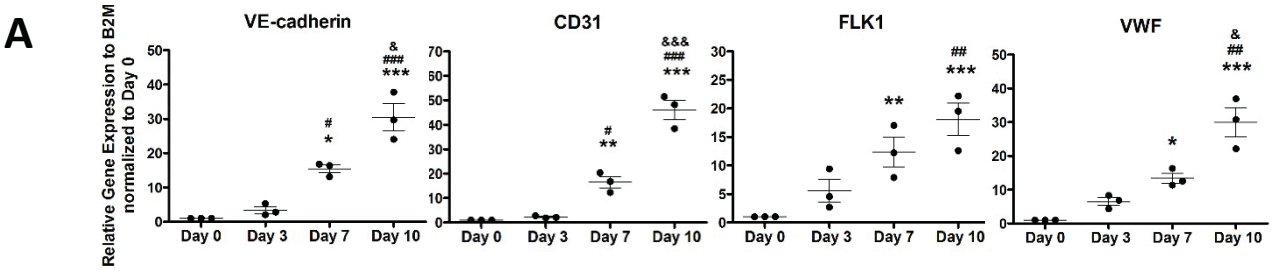


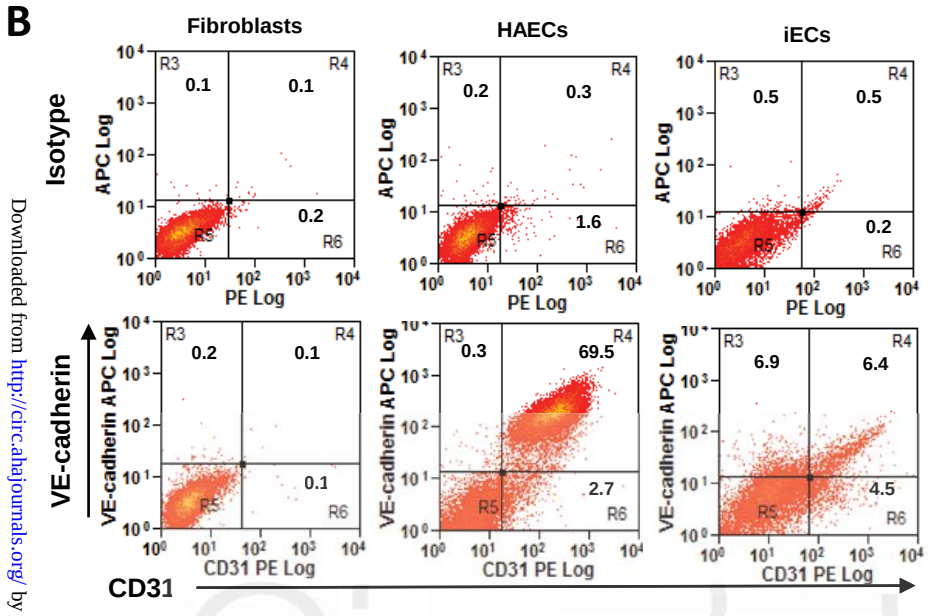


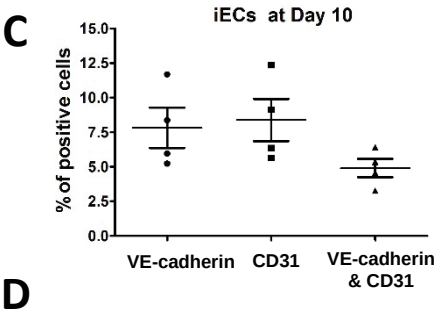


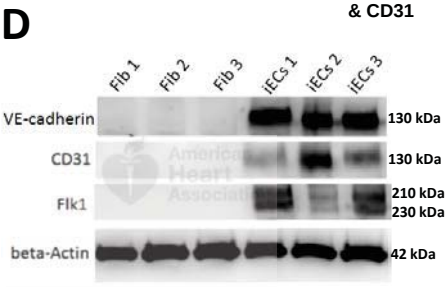


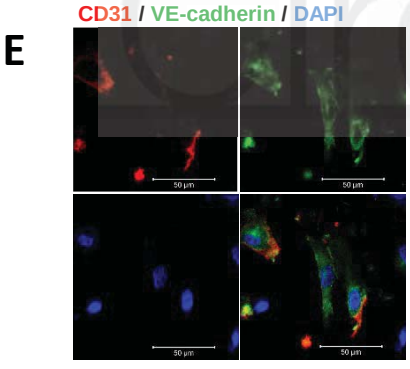


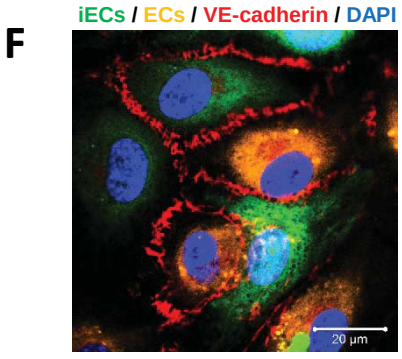


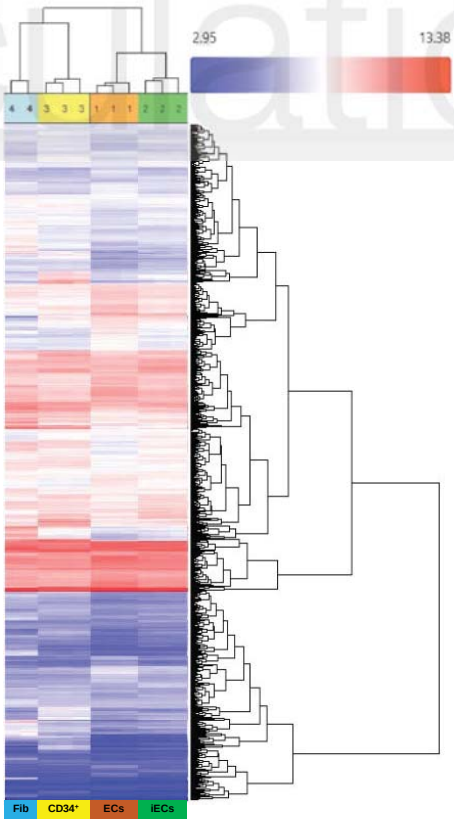


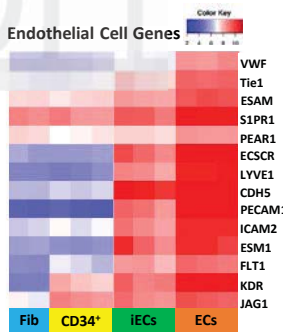


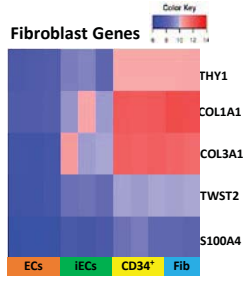

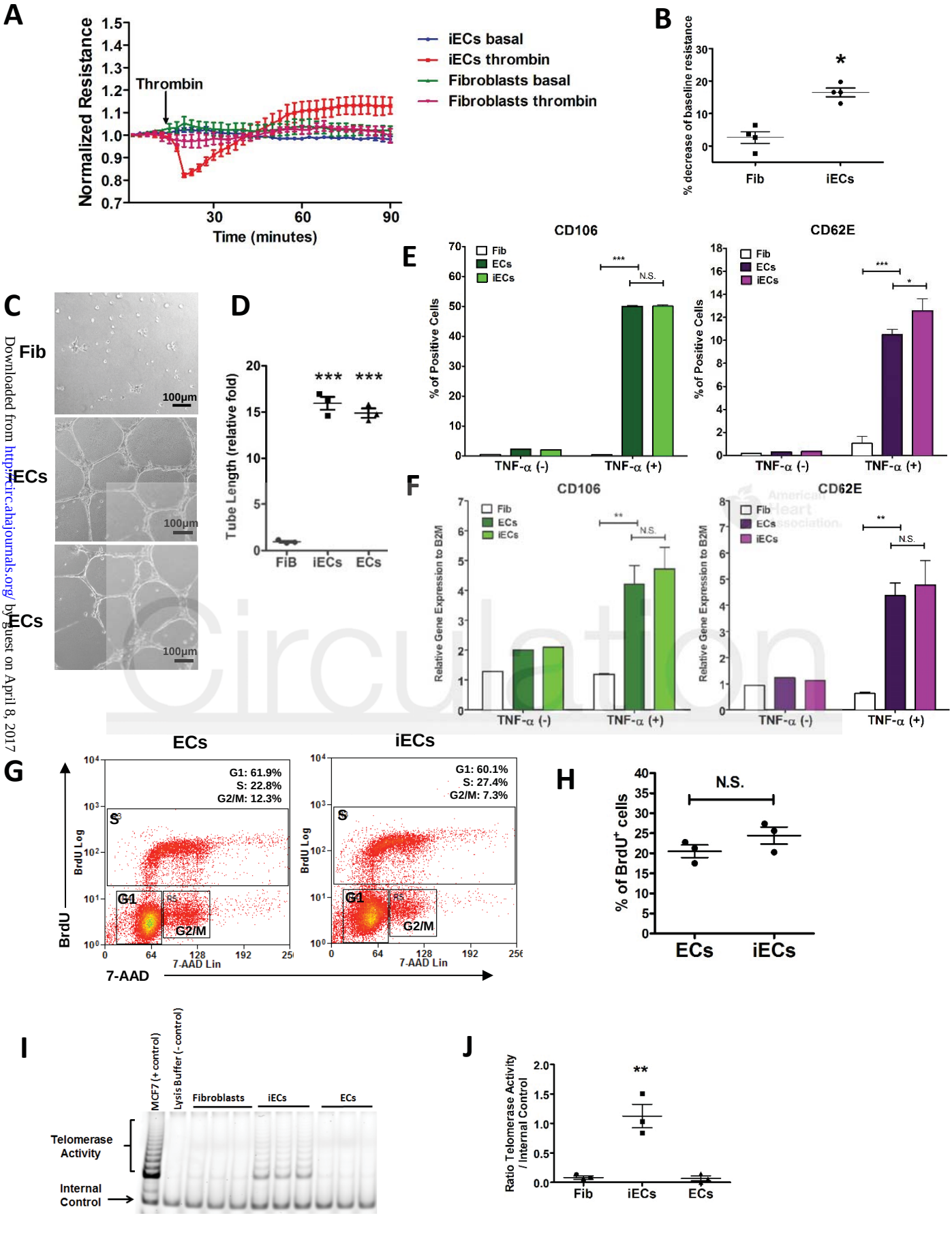

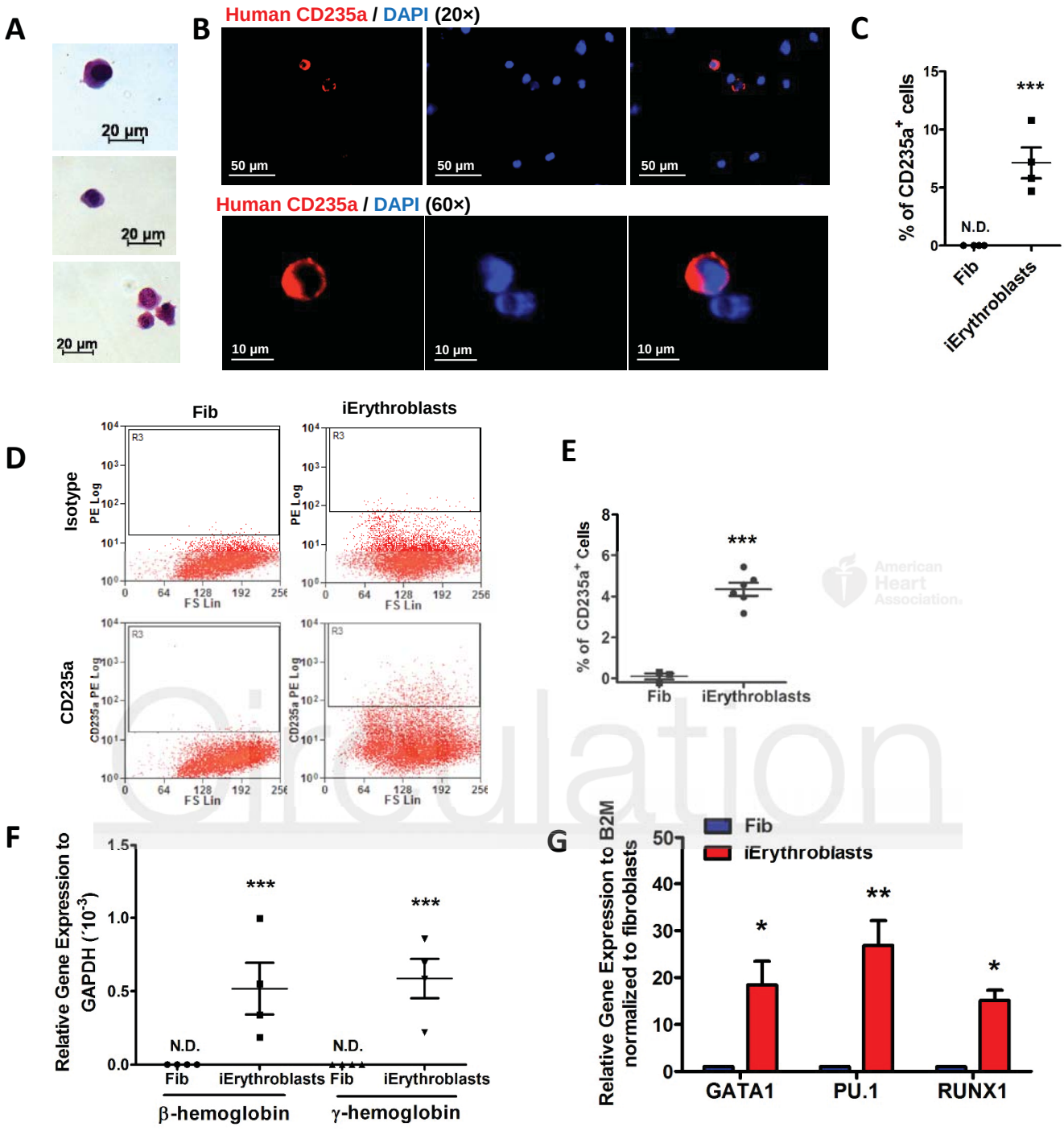

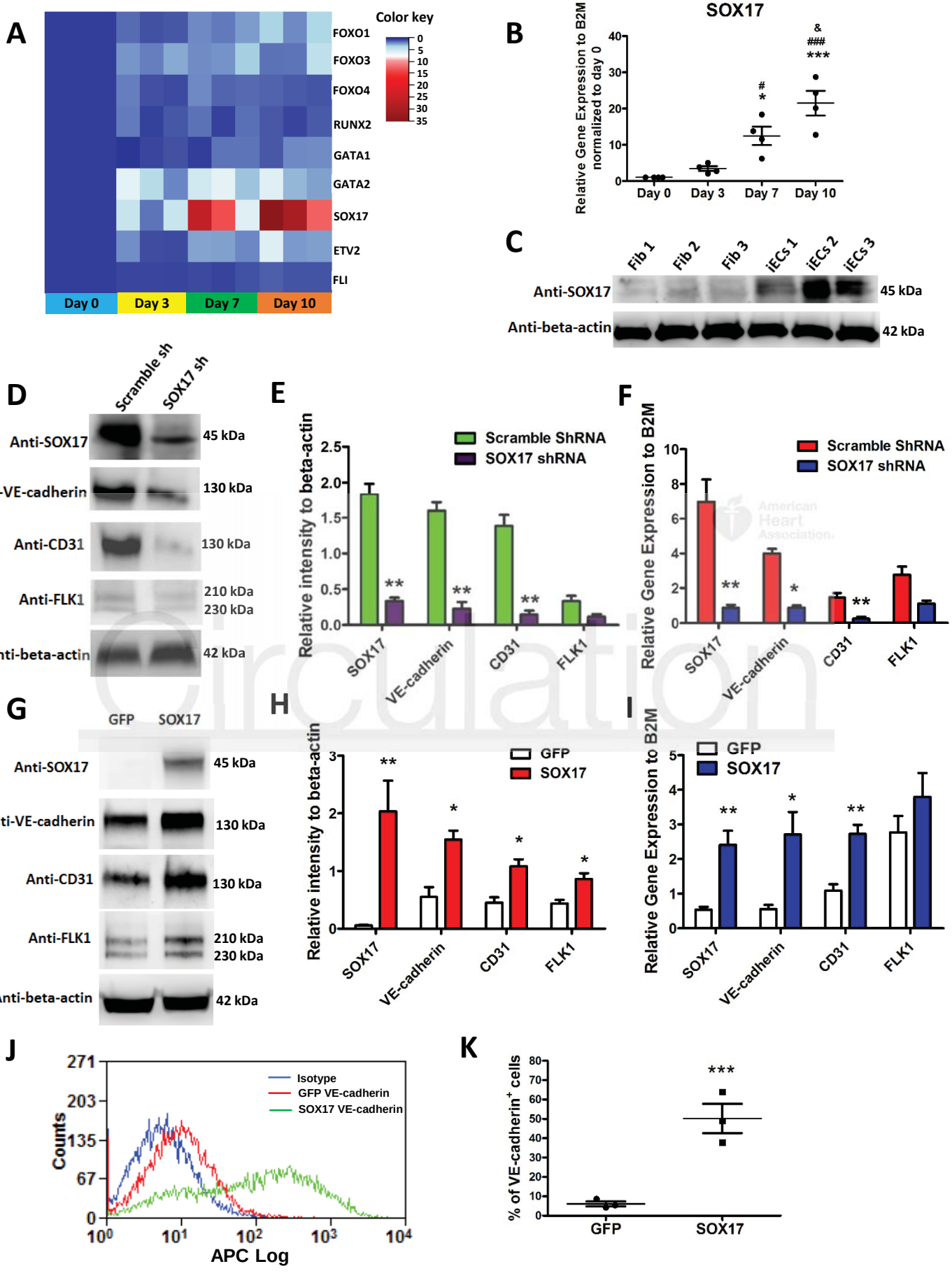

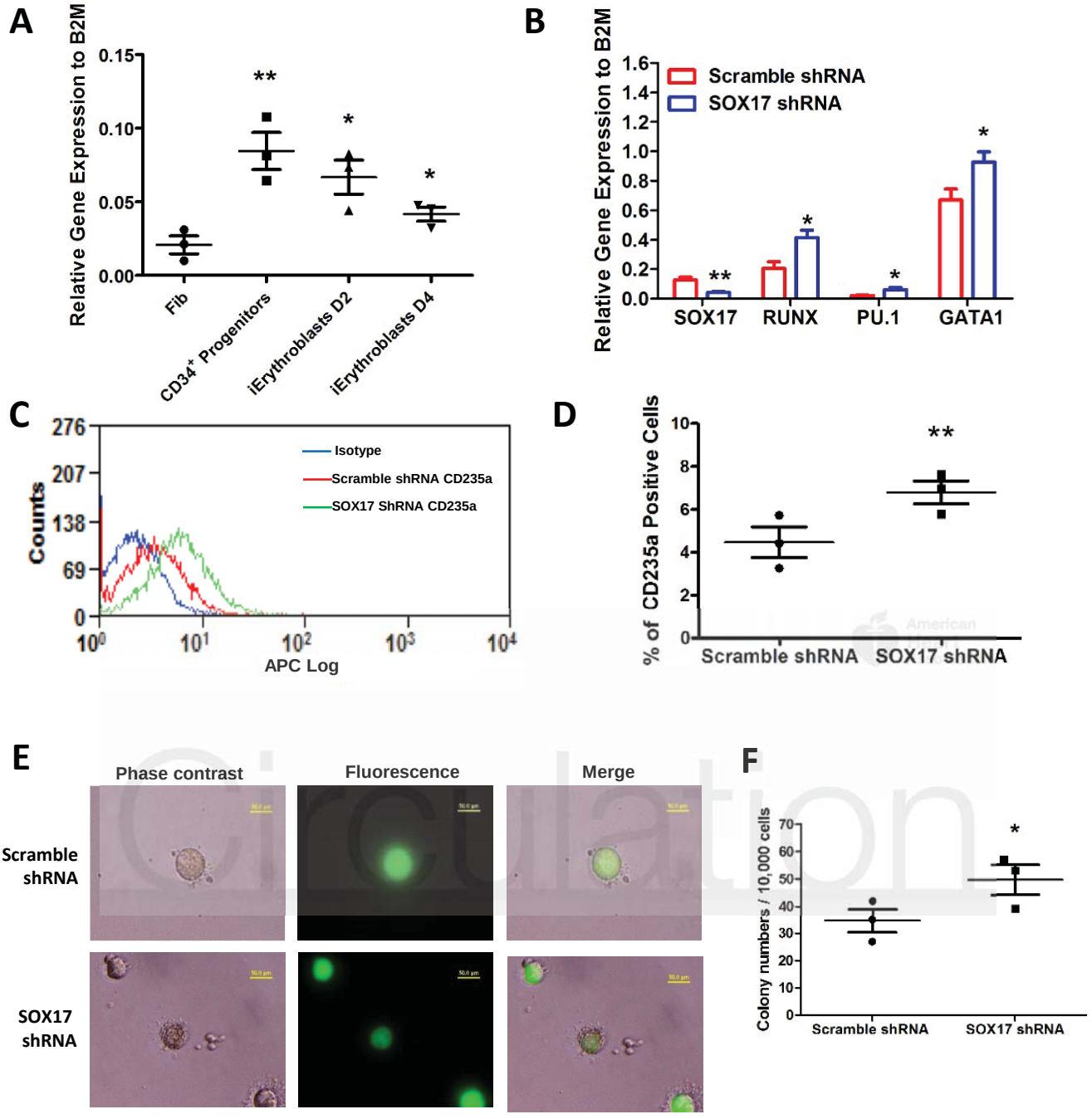

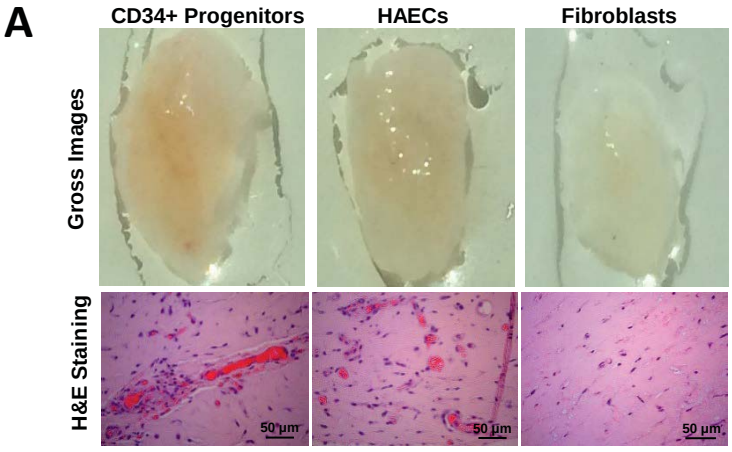


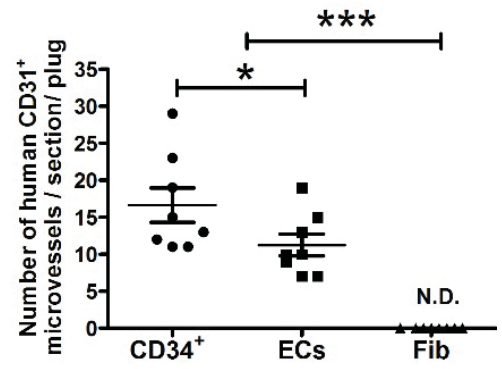


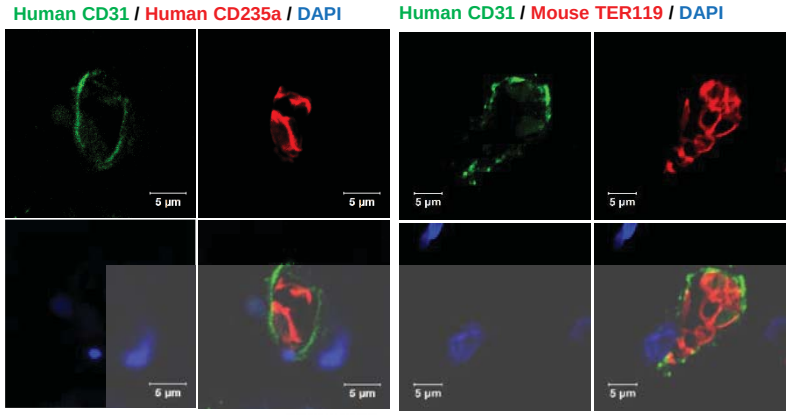


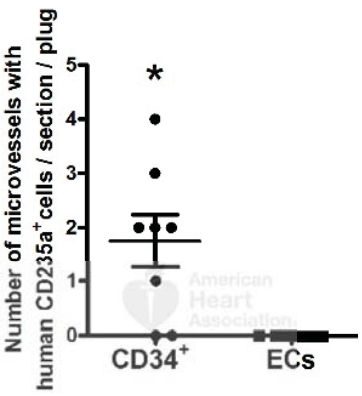


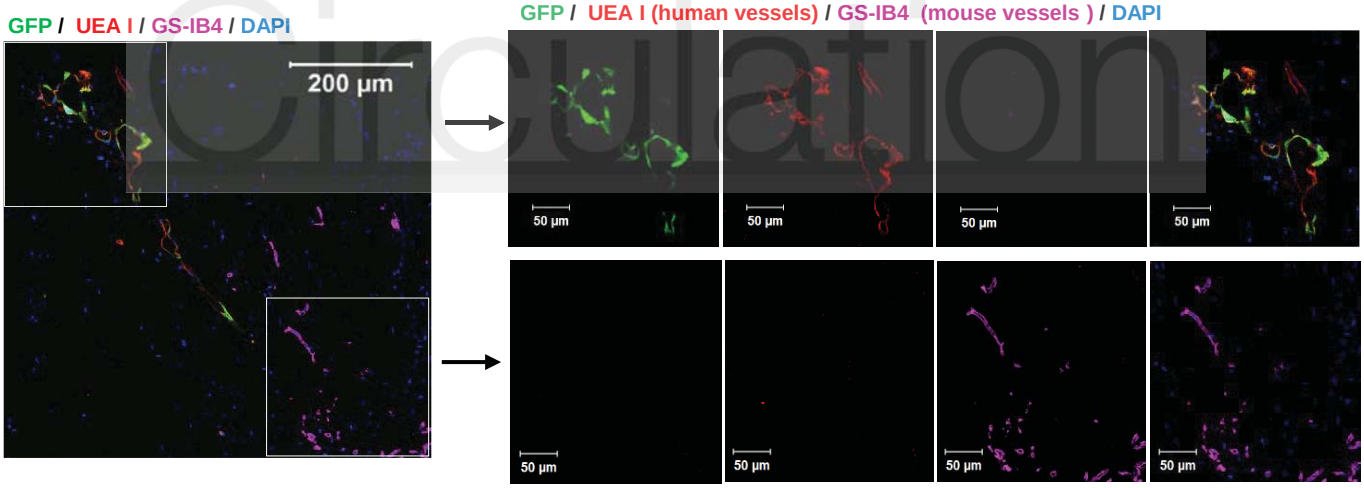


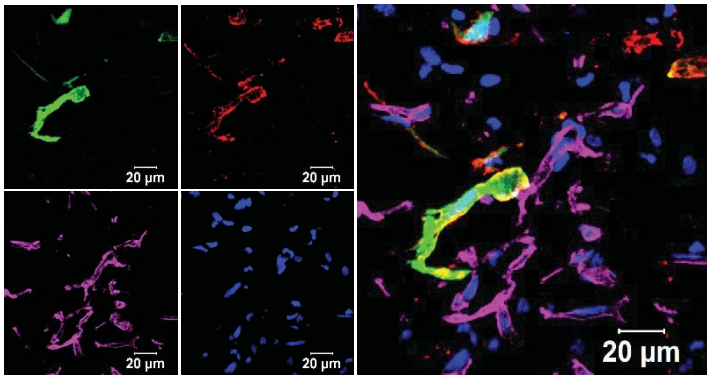


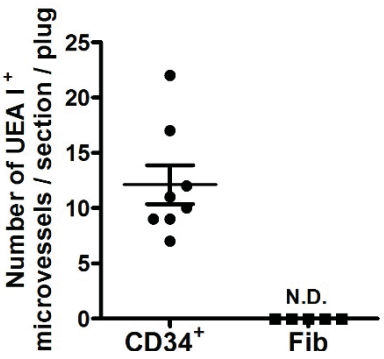

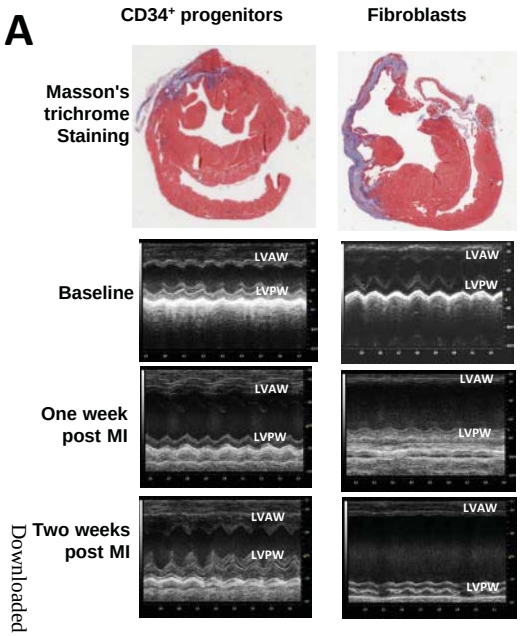


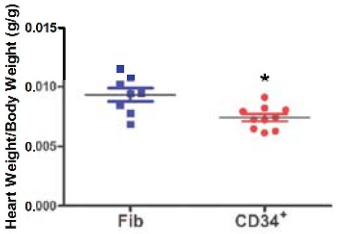


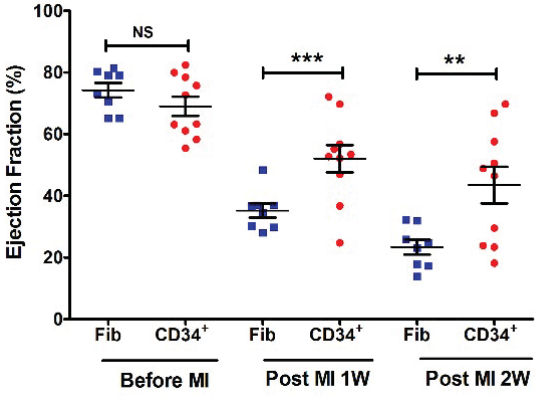


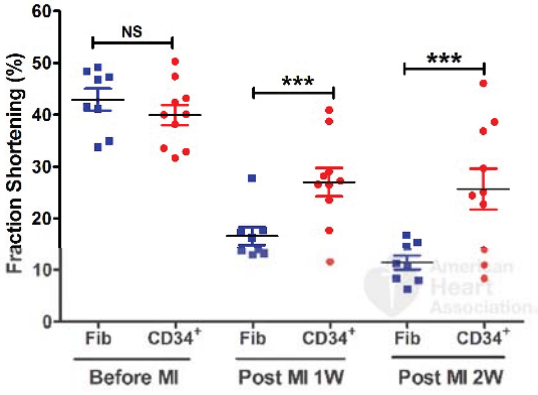


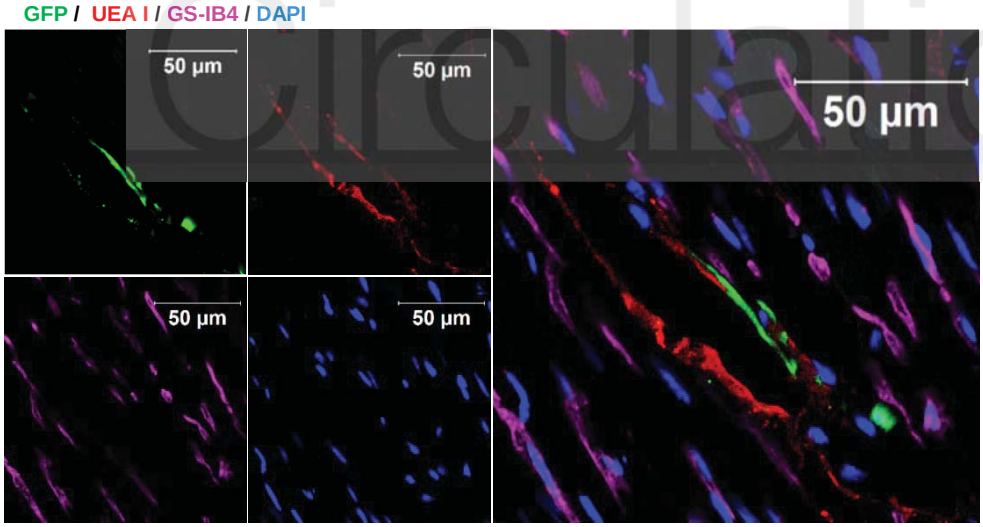


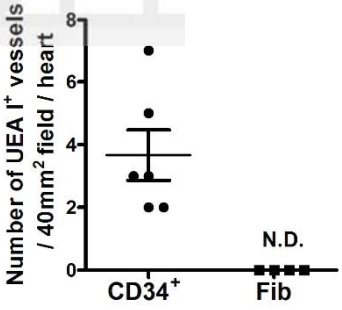


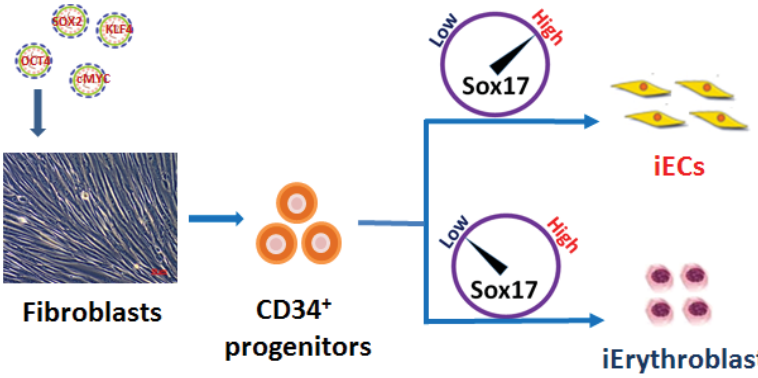

# SOX17 Regulates Conversion of Human Fibroblasts into Endothelial Cells and Erythroblasts via De-Differentiation into CD34 $^{+}$ Progenitor Cells

Lianghui Zhang, Ankit Jambusaria, Zhigang Hong, Glenn Marsboom, Peter T. Toth, Brittney-Shea Herbert, Asrar B. Malik and Jalees Rehman

*Circulation.* published online April 5, 2017;
*Circulation* is published by the American Heart Association, 7272 Greenville Avenue, Dallas, TX 75231

Print ISSN: 0009-7322. Online ISSN: 1524-4539

**SUPPLEMENTAL MATERIAL**

**Expanded Methods**

**Plasmids and retroviral or lentivirus constructs**. The small double-stranded hairpin shRNAs targeting SOX17 were designed by BLOCK-iT RNAi Designer (Invitrogen), synthesized by Integrated DNA Technologies (IDT), and inserted into a pLL3.7 lentiviral vector [1]. The sequences of SOX17 shRNAs were SOX17-1: GGACCGCACGGAATTTGAA; SOX17-2: GCATGACTCCGGTGTGAAT; SOX17-3: CCGCGGTATATTACTGCAA. Lipofectamine 2000 was used to transfect pLL3.7 lentiviral vector to HEK293T cells (seed $2.0 \times 10^6$/6-well dish 1 day prior). The medium containing lentiviruses was collected and filtered 2 days after transfection. The iECs was incubated with the virus cocktail supplemented with 8μg/ml polybrene for 6-8hr. To overexpress SOX17 and distinguish overexpressed genes from endogenous gene expression, full-length SOX17 (pMXs-SOX17) plasmids were purchased from Addgene (Cat: 50781 and 50782 respectively). To package retrovirus expressing SOX17, Fugene HD transfection reagent (Roche, E2311) was used to transfect PLAT-A cells ($1.0 \times 10^6$ / 6-well dish). The medium containing the retrovirus was collected and filtered 2 days after transfection. For SOX17, over-expression studies, iECs were incubated with a virus cocktail supplemented with 4μg/ml polybrene for 6-8hr.

**Quantitative real-time PCR.** Total RNA was extracted using the PureLink RNA Mini Kit (Ambion) according to manufacturer's protocol. cDNA was synthesized by High Capacity cDNA Reverse Transcription Kit (Applied Bipsystems). 50ng cDNA (relative to RNA amount) was amplified by real-time PCR. FastStart Universal SYBR Green Mastermix (Roche) was used for quantitative real-time PCR. TaqMan® Gene Expression Assays

from Applied Biosystems were used to detect human hemoglobin beta and human hemoglobin gamma with the primer/probe sets of hemoglobin beta (Hs00747223_g1) and hemoglobin gamma (Hs00361131_g1), respectively, while GAPDH (Hs02758991_g1) served as control. The sequences of qPCR primers are shown as following:

| | | | |
|---|---|---|---|
| Human | *B2M`* | Forward | 5'- ATAAGTGGAGGCGTCGCGCTG |
| | | Reverse | 5'- ACAGCTAAGGCCACGGAGCG |
| Human | *CD34* | Forward | 5'- CCACAGGAGAAAGGCTGGGCG |
| | | Reverse | 5'- CCGGTCCCGTTTTCCTGAGCC |
| Human | *OCT4* | Forward | 5'- AGAAGGATGTGGTCCGAGTGTG |
| | | Reverse | 5'- CATAGTCGCTGCTTGATCGC |
| Human | *c-MYC* | Forward | 5'- AAGACAGCGGCAGCCCGAAC |
| | | Reverse | 5'- TGGGCGAGCTGCTGTCGTTG |
| Human | *NANOG* | Forward | 5'- ACAACTGGCCGAAGAATAGCA |
| | | Reverse | 5'- GGTTCCCAGTCGGGTTCAC |
| Human | *VE-cadherin* | Forward | 5'- GACCGGGAGAATATCTCAGAGT |
| | | Reverse | 5'- CATTGAACAACCGATGCGTGA |
| Human | *CD31* | Forward | 5'- AACAGTGTTGACATGAAGAGCC |
| | | Reverse | 5'- TGTAAAACAGCACGTCATCCTT |
| Human | *FLK1* | Forward | 5'- TCGAAGCATCAGCATAAGAAACTT |
| | | Reverse | 5'- GCCCACTGGATGCTGCA |
| Human | *VWF* | Forward | 5'- GGGCTGCCAGAAACGCT |
| | | Reverse | 5'- CAAGATACACGGAGAGGCTCACT |
| Human | *SOX17* | Forward | 5'- TCTGCCTCCTCCACGAAG |
| | | Reverse | 5'- ACGCCGAGTTGAGCAAGA |
| Human | *GATA1* | Forward | 5'- ATCAAGCCCAAGCGAAGACT |
| | | Reverse | 5'- CATGGTCAGTGGCCTGTTAAC |
| Human | *PU.1* | Forward | 5'- GGGGTGGAAGTCCCAGTAAT |
| | | Reverse | 5'- ACGGATCTATACCAACGCCA |

| | | | |
|---|---|---|---|
| Human | *RUNX1* | Forward | 5’- AGAACCTCGAAGACATCGGC |
| | | Reverse | 5’- GGCTGAGGGTTAAAGGCAGTG |

**Flow cytometry**. Cells were harvested from culture dishes and analyzed on the CyAn ADP instrument (Beckman Coulter) with Summit software 4.4. The antibodies used for flow cytometry analysis were CD34-PE (130-081-002, Miltenyi Biotec), Alexa Fluor 647 mouse anti-human CD144 (561567, BD Biosciences), FIFC anti-hCD31/PECAM-1 (FAB3567P, R&D Systems), Alexa Fluor 647 mouse anti-human CD309 (VEGFR-2) (560495, BD Biosciences), PE mouse anti-human CD106 (555647, BD Biosciences), and APC mouse anti-human CD62E (551144, BD Biosciences), APC mouse anti-human CD235a, (MACS 130-100-262), PE mouse anti-human CD235a (BD Biosciences 555570), PE mouse anti-human TRA-160 (eBioscience, 12-8863) , and PE mouse anti-human TRA-180 (eBioscience, 12-8883). Isotype controls were Alexa Fluor 647 mouse $IgG1_k$ (557714, BD Biosciences), Alexa Fluor 647 mouse $IgG1_k$ (557783, BD Biosciences), PE mouse $IgG1_k$ (554680, BD Pharmingen), PE mouse $IgG2b_k$ (555743, BD Biosciences). FITC mouse $IgG1_k$ (554008, BD Pharmingen) and APC mouse $IgG2a_k$ (555576, BD Biosciences). Cell proliferation was assayed by flow cytometry using the APC BrdU flow cytometry kit (51-9000019AK, BD Biosciences) according to manufacturer’s instructions.

**Cytospin preparation and Hema 3 staining.** Cells ($10^5$) were suspended in 300 ml and used for cytospin preparations with the Thermo Scientific Shandon 4 Cytospin kit. The slides were fixed and stained with Hema 3 kits (Fisher Scientific, 123-869) according to manufacturer’s protocol to visualize erythroblasts. The cells were imaged using a Zeiss ApoTome inverted microscope with 20×, 40× and0× objectives.

**Erythroid Colony-Forming assay.** MethCult™ H4034 Optimum with Recombinant Cytokines and EPO were purchased from Stemcell Technologies and colony forming assay to evaluate the colony-forming function of generated erythroblasts were performed according to the manufacturer instructions. Briefly, $3\times10^3$ induced erythroblasts or fibroblasts were collected, washed and then mixed in 3×1,300 µL MethCult™. The suspended cells were dispensed into petri-dishes using a syringe and blunt-end needle. The dishes were then incubated for 14 days in a humidified incubator at 37°C and 5% CO2. The erythroid colonies were evaluated and counted using an inverted microscope and gridded scoring dishes. The colonies were plucked for further assays.

**Immunocytochemistry, immunohistochemistry and fluorescence microscopy.** Immunocytochemistry was performed on cells after fixation with 4% paraformaldehyde. Fixed cells were permeabilized and blocked with 5% normal goat serum, 0.1% Triton X-100 in PBS for 30 min at RT [2]. Then the cells were incubated with primary antibodies for 2hr and secondary antibodies labeled with fluorescence Alexa488 and Alexa647 (Invitrogen, Carlsbad, CA) for 1hr. Immunohistochemistry was performed on paraffin-embedded sections after heat-induced antigen retrieval (30 min at 95ºC in 0.01M sodium citrate, pH6). The slides were permeabilized and blocked with 5% normal goat serum, 0.1% Triton X-100 in PBS for 1hr at RT. The slides were then incubated with primary antibody at 4ºC overnight. For immunofluorescence, fluorescent Alexa Fluor-488 and Alexa-568 (Invitrogen, Carlsbad, CA) labeled secondary antibodies were applied to identify the primary antibodies. The slides were mounted in ProLong Gold antifade reagent with DAPI (Invitrogen). Florescence images were acquired using Zeiss ApoTome microscope with 20×, 40× and 60× objectives. Confocal image acquisition was performed

using a Zeiss LSM 780 laser scanning microscope (Carl Zeiss Jena) with 20×, 40× and 60× water objectives. Primary antibodies used were mouse anti-human CD31 (M-0823, DAKO, Denmark), goat anti-VE-cadherin (Santa Cruz Biotech, SC-6458), rat anti-mouse TER-119/Erythroid cells (BD Pharmingen, 550565), mouse anti-human CD235a (Glycophorin A) (R&D Systems, MAB 1228), mouse anti-human CD235a (R&D Systems, MAB 1125).

**Western blotting.** Immunoblotting was performed as described [2]. The primary antibodies applied in Western blotting were mouse anti-actin (A2066, Sigma); goat anti-VE-cadherin (sc-6458, Santa Cruz); rabbit anti-FLK1 (VEGFR2) (2479, Cell Signaling Technology), mouse anti-human CD31 (M-0823, DAKO, Denmark), goat anti-human SOX17 (AF1924, R&D). Donkey horseradish peroxidase (HRP)-linked anti-goat, mouse and rabbit IgG (SantaCruz) were used as secondary antibodies. Signals were developed by enhanced chemiluminescence HRP substrate – SuperSignal West Femto Maximum Sensitivity Substrate (34095, Thermo Scientific) and detected with the LAS-3000 mini (Fuji).

**Transendothelial electrical resistance measurements.** Assessment of responses of iEC to inflammatory stimuli was performed by measuring thrombin-induced increase in endothelial permeability as described [3]. Human iECs and control human EC ($5.0\times 10^4$/ $cm^2$) were cultured on gelatin-coated gold electrodes for 1 day. The smaller electrode and larger counter electrode were connected to a phase-sensitive lock-in amplifier to monitor the voltage. A constant current of 1 μA was supplied by a 1 V, 4000 Hz AC signal connected serially to a 1MΩ resistor between the smaller electrode and the larger counter electrode. Before each experiment, confluent endothelial monolayers using both cell types were incubated in serum-free medium for 1hr. Thrombin (3.5μg/ml - 0.5 Units) was

added as indicated. The data are presented as a change in the resistive portion of electrical impedance normalized to its value at time 0.

**Gene expression and bioinformatics.** Gene expression data on fibroblasts, erythro-angioblasts derived from fibroblast de-differentiation, iECs, and adult human ECs were obtained using the Affymetrix GeneChip® Human Transcriptome Array 2.0. The analysis was performed in the R environment for statistical computing using the Affy and Limma packages. The 11 Affymetrix CEL files were pre-processed by Robust MultiChip Analysis. For each gene, the normalized intensity in each cell type was paired with the normalized intensity of the remaining samples and analyzed with the Limma package. A linear model was fitted to the design matrix for the samples using Limma, and differentially expressed genes identified for each pairwise comparison using a moderated *t* statistic, which applies an empirical Bayes method to borrow information across genes. P-values were adjusted for multiple testing using the Benjamini and Hochberg's method, which controls the false discovery rate. Gene expression profiles were visually depicted using heatmaps. Samples and genes were ordered by hierarchical clustering and represented by the dendrogram. The color bar indicates gene expression level in binary logarithm ($log_2$) scale. The blue to red color spectrum represented low to high expression levels.

**Tube formation assay**. A cell suspension containing $0.3\times10^5$/ well of either ECs (control) or iECs was placed on top of wells coated with Matrigel (10 mg/ml; BD Matrigel Basement Membrane Matrix, A6661) in a 24-well plate (Nunc). Rearrangement of cells and formation of capillary structures were observed at 24 hours.

**Telomerase activity assay.** Telomerase activity was determined using the telomeric repeat amplification protocol (TRAP). TRAP assay was performed using the TRAPeze

Telomerase Detection kit (Millipore) and a Cy5 fluorescently labeled TS primer according to established protocols [4]. Densitometry of telomerase-specific ladder and internal standard were quantified using ImageJ and used to calculate relative telomerase activity compared to an internal standard control.

**In vivo staining of functional human and mouse vessels by lectins.** Rhodamine-labeled Ulex Europaeus Agglutinin I (UEA I; vectorlabs, DL-1208 for staining human endothelium) and DyLight 649 labeled Griffonia Simplicifolia Lectin I isolectin B4 (GS-IB4, vectorlabs, RL-1062 for staining mouse endothelium) were mixed into saline with 1 mM CaCl2 solution as described [5]. The lectin mixture (50 μg of each/100 μL/mouse) [5] was injected intravenously 30 minutes before harvesting Matrigel implants or hearts. Quantification of vessel density in plugs and hearts was described as above.

**Teratoma formation assay.** $1\times10^6$ $CD34^+$ progenitor cells or iPSCs suspended in Matrigel were injected subcutaneously to the abdomen of anesthetized immune-deficient NOD-SCID mice (Jackson Laboratory, NOD.Cg-*Prkdc*$^{scid}$ *Il2rg*$^{tm1Wjl}$/SzJ, strain 005557). The iPSCs were generated from reprogramming human BJ newborn foreskin fibroblasts (ATCC, Manassas, VA) using a protocol previously described. The mice were monitored for 8 weeks. The mice were sacrificed and teratomas or plugs were explanted at 8 weeks' post implantation. The teratoma were fixed in 10% formalin for 2 days and embedded in paraffin. Histological characterization of H&E staining slides was performed to identify the cells from all three germ layers.

**Myocardial infarction surgery** Anesthesia was introduced with 1.5-3% isoflurane inhalation in a closed glass chamber and Etomidate (10 mg/kg body weight IP). Mice were orally intubated with one 18G angiocath sleeve and artificially ventilated with a rodent

respirator (tidal volume 0.2-0.3ml (based on body weight), rate 135 strokes/min). Surgical anesthesia was maintained using 1% isoflurane delivered through a vaporizer with air connected in series to rodent ventilator. A dose of buprenorphine sustained release (0.1 mg/kg SC) was administered pre-operatively. Under microscopic view, left thoracotomy was performed by 1 cm careful incision along sternum and 1 mm to the left from a midline between the 2nd and 4th rib in layers (skin, pectoral muscles and ribs avoiding mammary arteries). Having the heart in view, the pericardium was removed to ligate the left main coronary artery with 8-0 prolene suture 1–2 mm below the ostium. The chest cavity was then closed in three layers: intercostal muscles-interruptive, pectoral muscles and skin-continuous with the 7-0 nylon sutures. The thorax was drained with a PE-10 cannula inserted into incision upon closure to evacuate the chest cavity and re-establish proper intrapleural pressure. After tube removal, mice were weaned from anesthesia and placed in the warming pad until ambulatory and then returned to the appropriate housing facility.

**Transthoracic echocardiography.** Evaluation of regional cardiac function based on LV thickness and morphology was performed by transthoracic echocardiography. Mice were anesthetized by 3.5% isoflurane and placed a heated platform (VisualSonics, Inc.) where ECG (lead II), heart rate, respiratory waveform and respiratory rate were monitored and displayed on the ultrasound's CPU display. Then, 3 views were recorded with the sample volume in the proper modes (B-mode, M-mode, pulsed Doppler or tissue Doppler): 1. The parasternal long axis [B-mode and/or M-mode]; 2. The parasternal short axis [M-mode was taken at the papillary level followed by tissue Doppler of the myocardium]; 3. Apical view [pulsed Doppler of the mitral flow]. Fractional shortening (FS) and ejection fraction (EF) were used as indices of cardiac contractile function. M-mode tracings were used to

measure LV internal diameter at end diastole (LVIDd) and end systole (LVIDs). FS was calculated according to the following formula: FS (%) = [(LVIDd − LVIDs)/LVIDd] × 100. EF is estimated from (LVEDV-LVESV)/LVEDV 100%. LVESV (left ventricular end systolic volume); LVEDV. (left ventricular end diastolic volume).

**SUPPLEMENTAL TABLE**

**Supplemental Table 1: Cardiac function assessment by echocardiography**

| Echo index | Treatment | Before MI | Post MI 1 W | Post MI 2 W |
|---|---|---|---|---|
| Heart Rate (bpm) | Fib | 443.99 ± 12.97 | 451.16 ± 27.41 | 455.33 ± 39.90 |
| | $CD34^+$ | 443.90 ± 12.97 | 491.61 ± 28.93 | 449.93 ± 24.67 |
| LV internal diameter at end systole (LVIDs) | Fib | 2.12 ± 0.13 | 3.60 ± 0.37 | 3.79 ± 0.53 |
| | $CD34^+$ | 2.01 ± 0.11 | 3.01 ± 0.27 | 3.46 ± 0.34 |
| LV internal diameter at end diastole (LVIDd) | Fib | 3.46 ± 0.11 | 4.56 ± 0.22 | 4.43 ± 0.27 |
| | $CD34^+$ | 3.26 ± 0.09 | 4.06 ± 0.64 | 4.03 ± 0.84 |
| LV End Systolic Volume (LVESV) (ul) | Fib | 12.56 ± 3.19 | 62.91 ± 5.20 | 79.96 ± 13.07 |
| | $CD34^+$ | 12.04 ± 3.27 | 34.55 ± 3.15 * | 56.43 ± 5.60 |
| LV End Diastolic Volume (LVEDV) (µl) | Fib | 48.49 ± 5.15 | 99.51 ± 12.96 | 114.4 ± 11.19 |
| | $CD34^+$ | 48.47 ± 5.95 | 70.29 ± 9.01 * | 93.36 ± 13.59 * |
| Stroke Volume (µL) | Fib | 35.74 ± 1.93 | 28.58 ± 3.49 | 24.49 ± 3.75 |
| | $CD34^+$ | 36.96 ± 1.51 | 36.32 ± 2.45 * | 37.58 ± 2.81 ** |
| Ejection Fraction (%) | Fib | 74.29 ± 2.36 | 35.19 ± 2.27 | 23.38 ± 2.39 |
| | $CD34^+$ | 69.04 ± 3.13 | 52.05 ± 4.42 *** | 43.50 ± 5.91 ** |
| Fractional Shortening (%) | Fib | 42.37 ± 5.29 | 16.07 ± 4.25 | 11.34 ± 3.89 |
| | $CD34^+$ | 39.95 ± 1.95 | 27.00 ± 2.74 *** | 25.66 ± 3.93 *** |
| Cardiac Output (ml/min) | Fib | 15.12 ± 0.4 | 12.41 ± 2.0 | 10.20 ± 1.01 |
| | $CD34^+$ | 15.57 ± 0.58 | 18.02 ± 1.2 ** | 15.80 ± 1.49 ** |
| LV Mass (mg) | Fib | 99.91 ± 7.24 | 155.20 ± 15.34 | 159.30 ± 16.67 |
| | $CD34^+$ | 94.29 ± 8.19 | 112.00 ± 12.70 * | 136.8 ± 9.47 |
| LV Mass Corrected (mg) | Fib | 70.60 ± 2.81 | 119.19 ± 11.10 | 131.48 ± 9.93 |
| | $CD34^+$ | 70.59 ± 2.30 | 84.22 ± 24.53 * | 86.18 ± 5.04 *** |

Data are presented as mean ± SE. ***P<0.001, **P<0.01, *P<0.05, $CD34^+$ progenitors ($CD34^+$) treatment were compared to fibroblasts (Fib) treatment using repeated measures

two-way ANOVA.

## Supplemental Figure 1

A

Fibroblasts

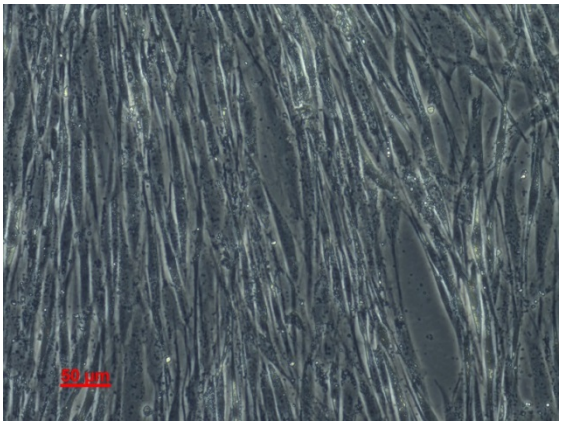


B

De-Differentiated
Fibroblasts at day 7

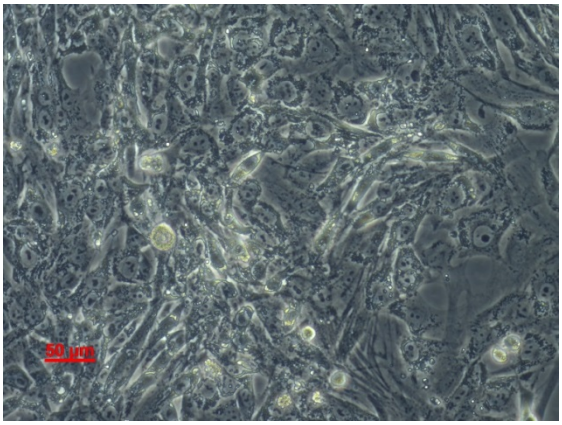


C

iECs at day 10

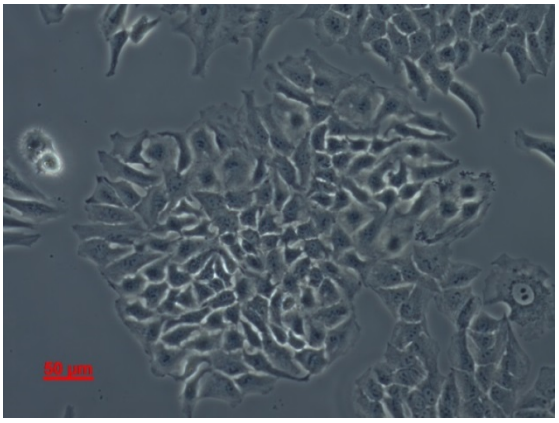


D

Induced Erythroblasts
at day 4

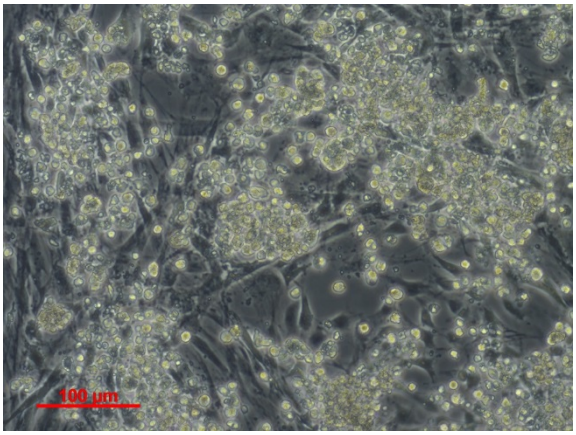


.

# Supplemental Figure 2

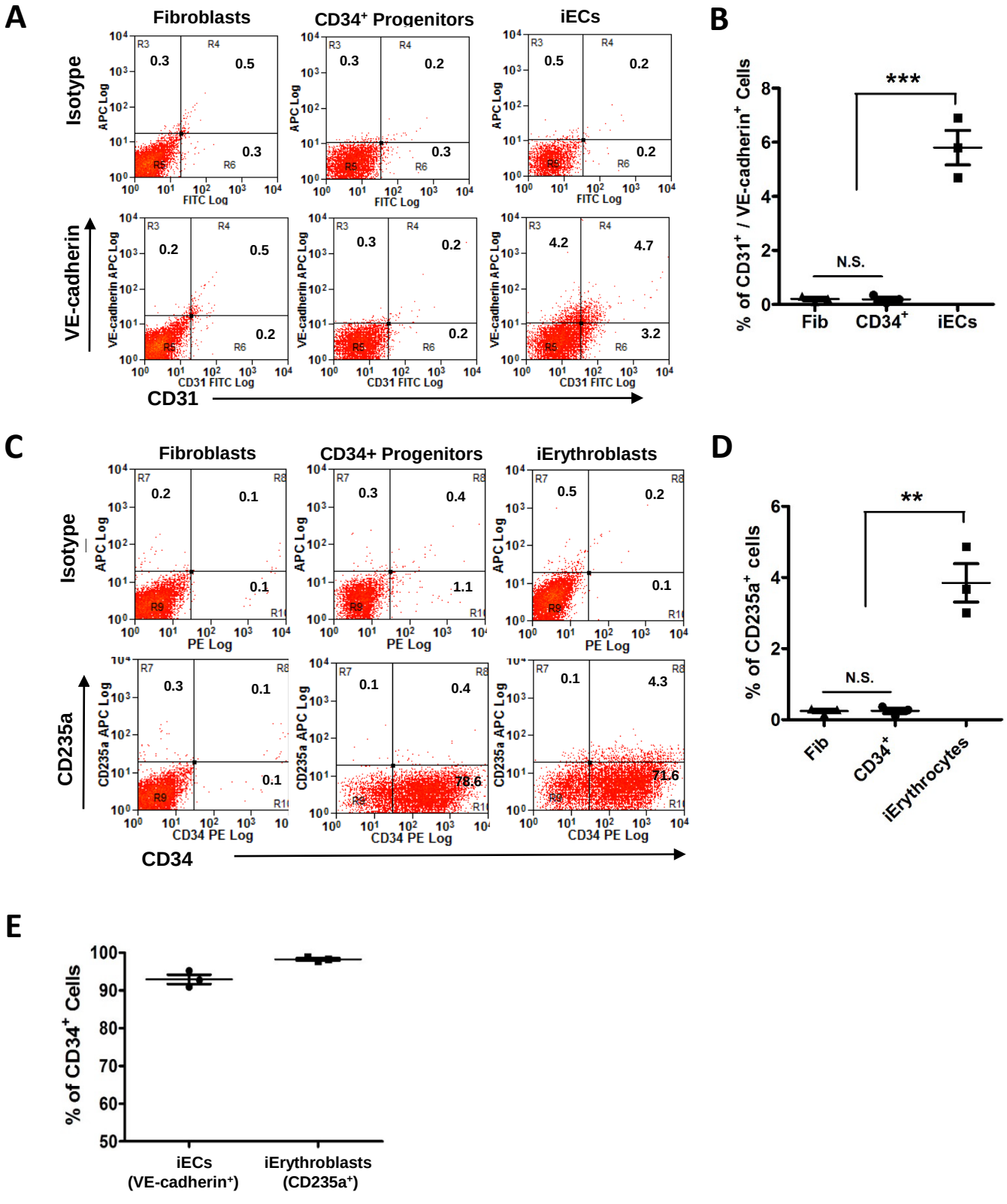

# Supplemental Figure 3

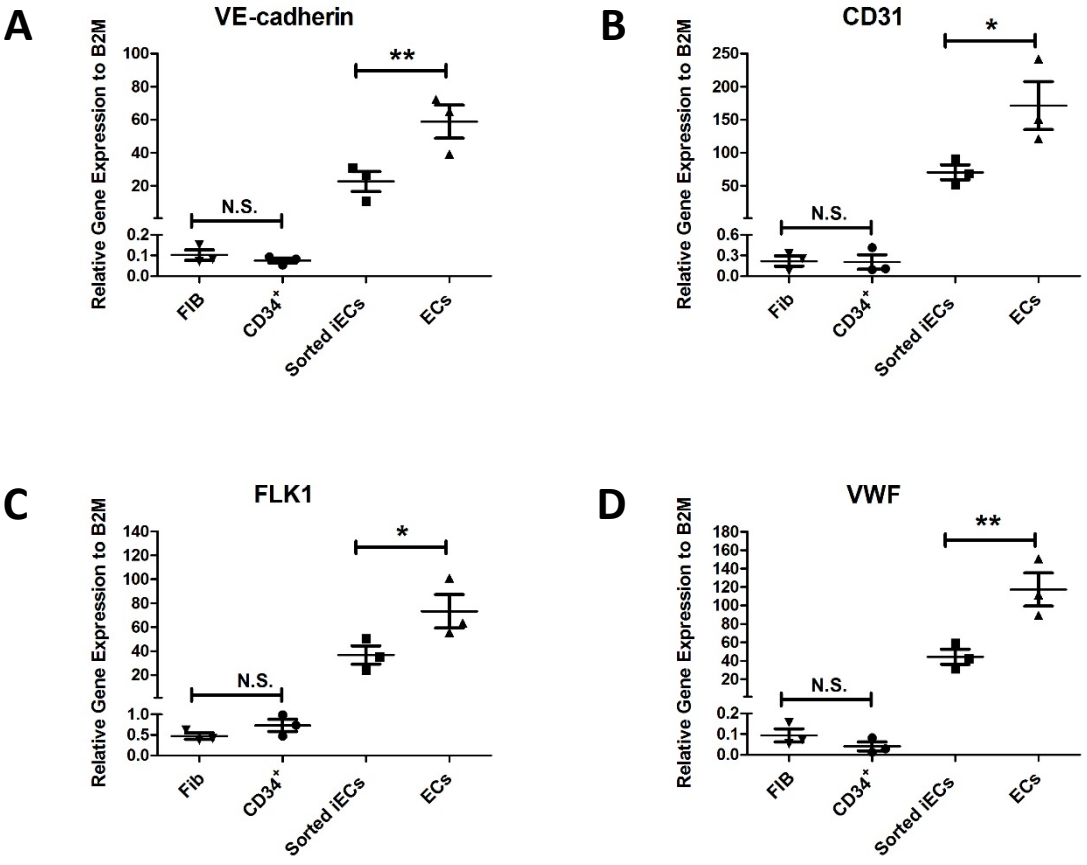

# Supplemental Figure 4

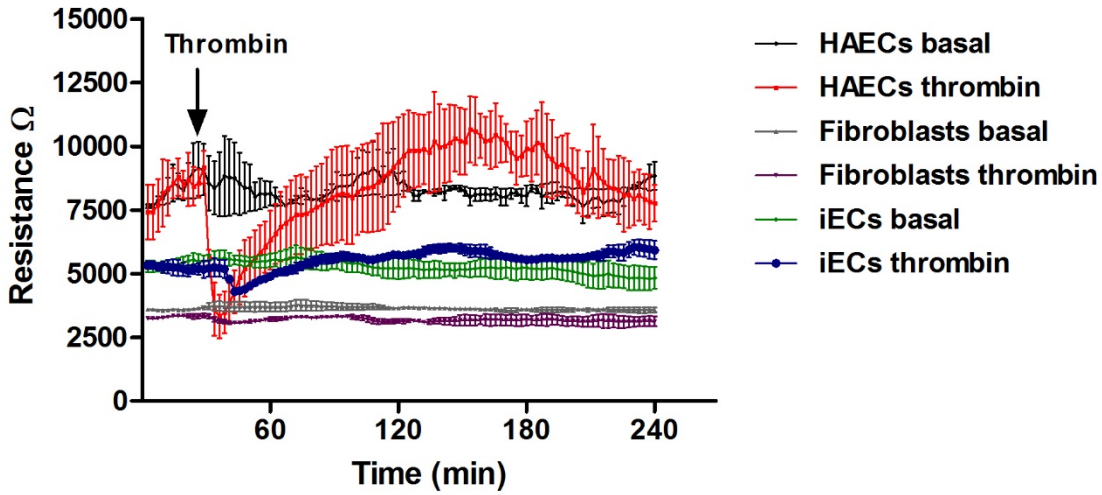

# Supplemental Figure 5

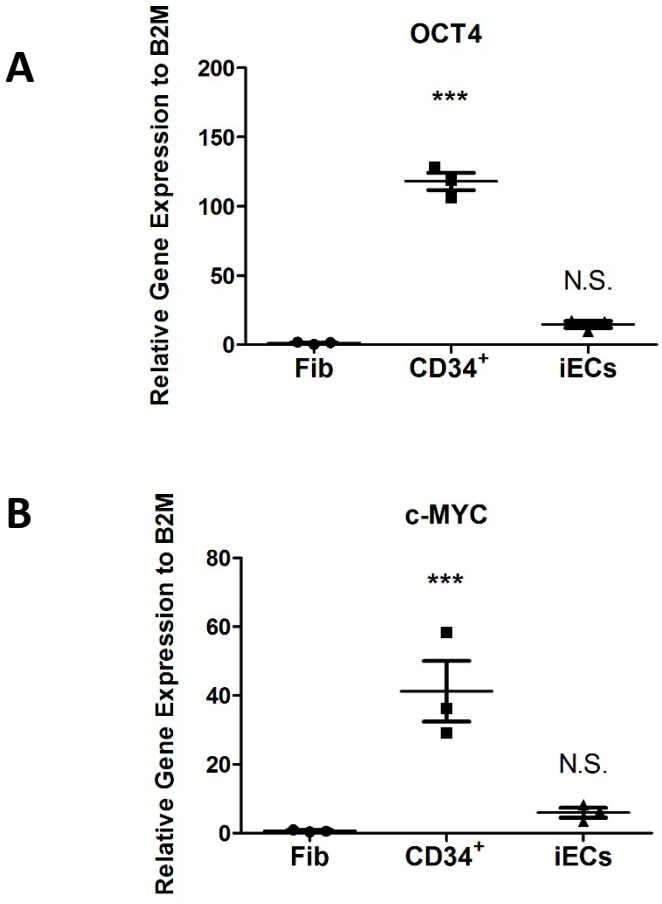

# Supplemental Figure 6

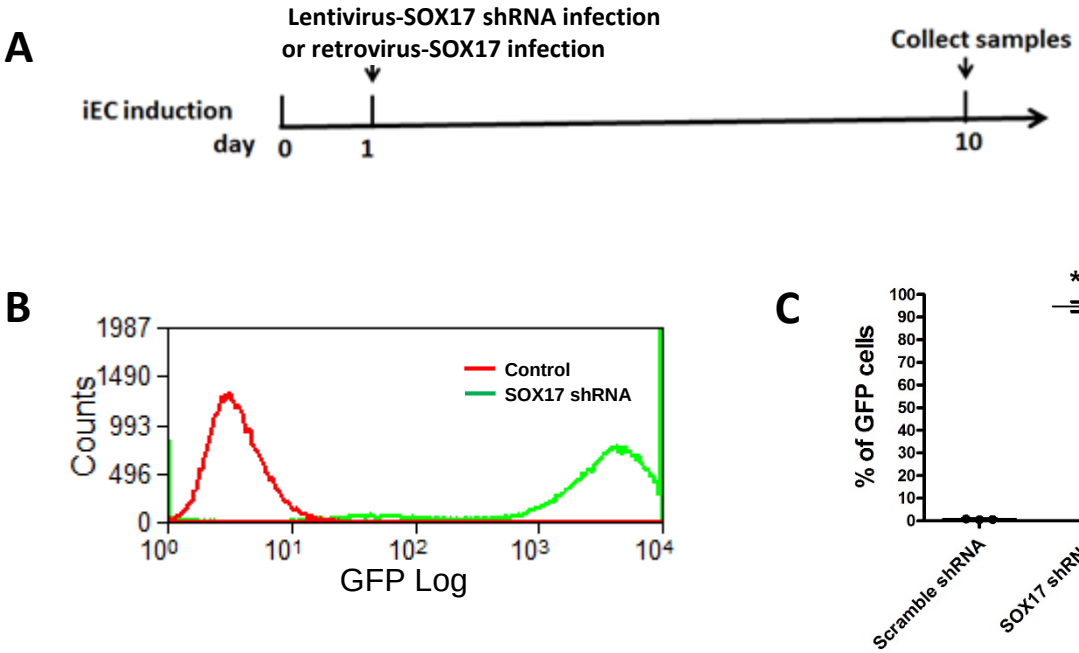


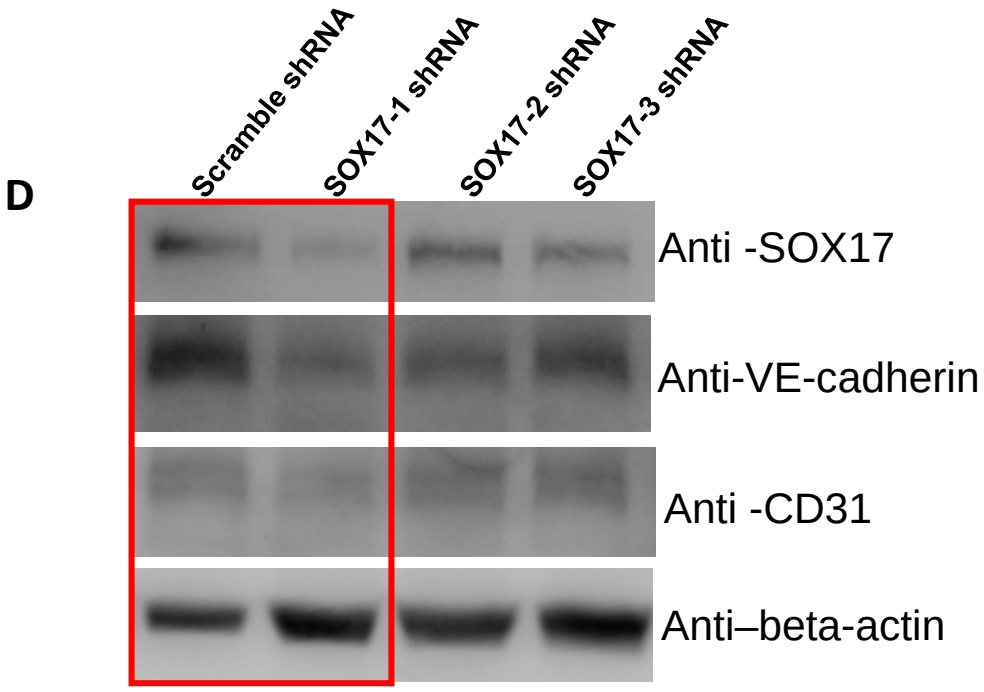

# Supplemental Figure 7

**A**

Mouse CD31 / Mouse TER119 / DAPI

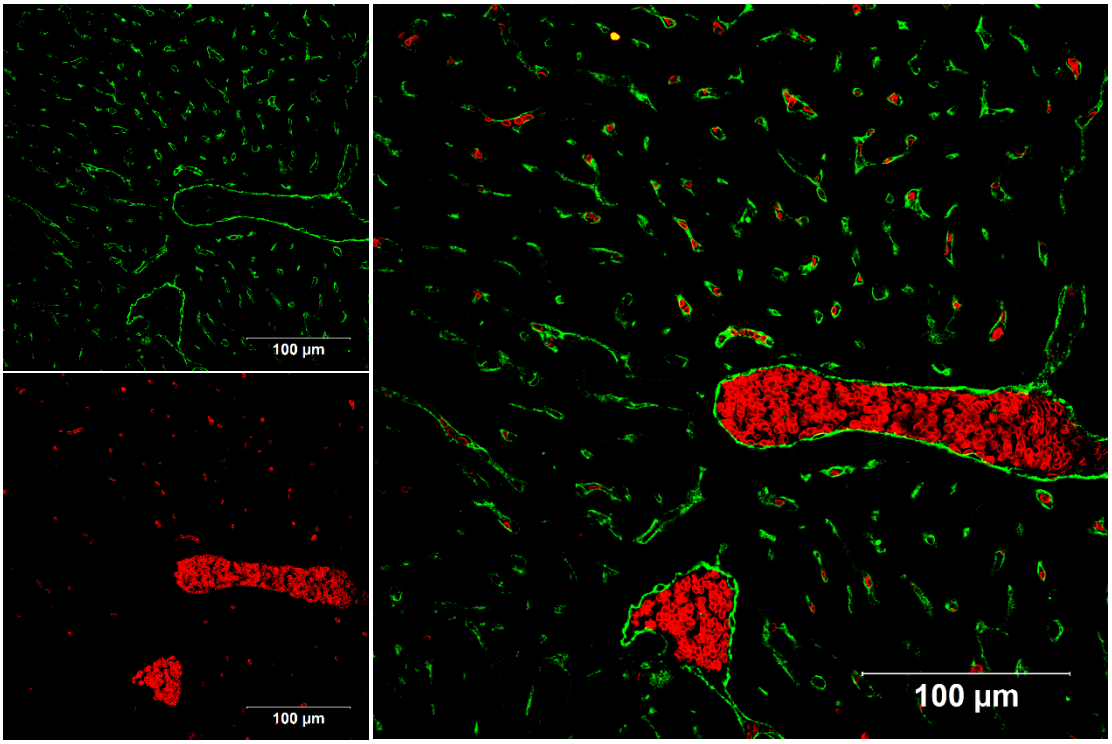


**B**

Mouse CD31 / Human CD235a / DAPI

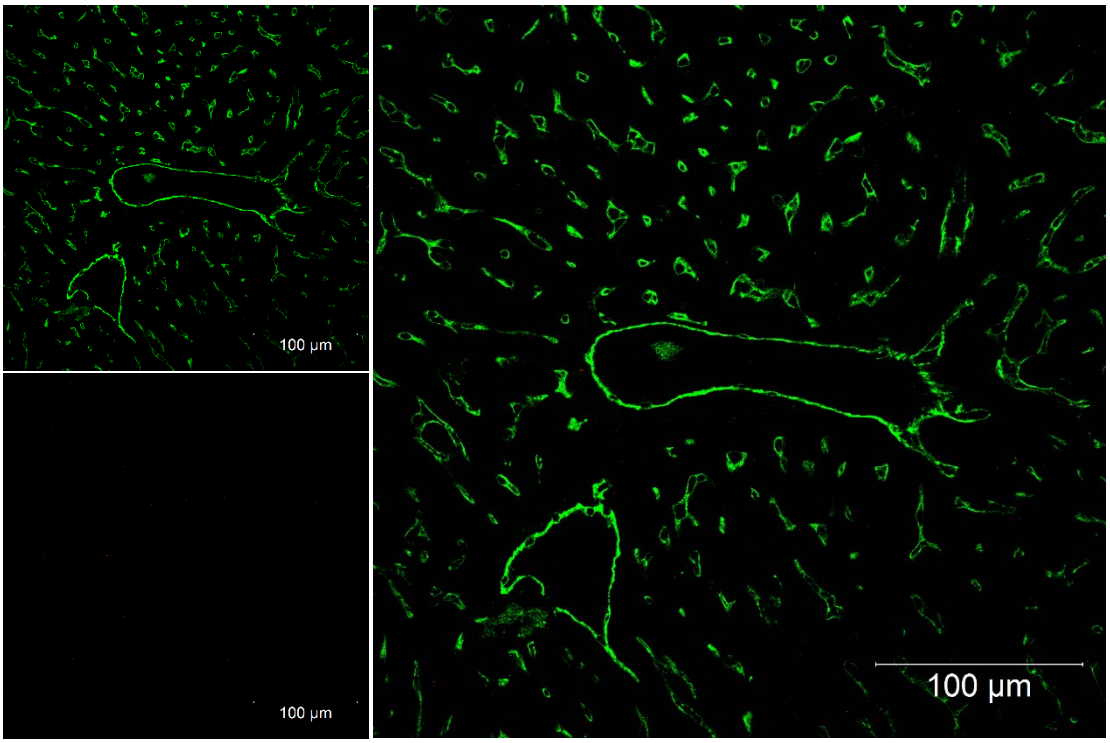

# Supplemental Figure 8

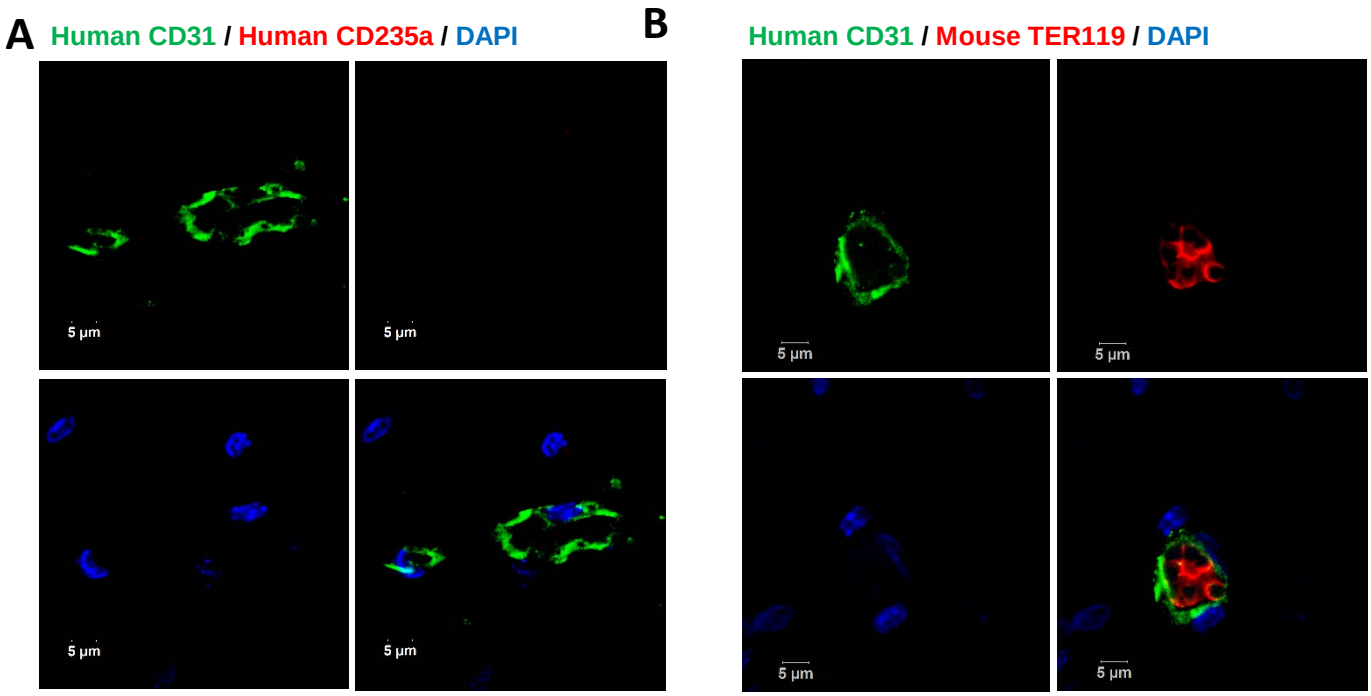

# Supplemental Figure 9

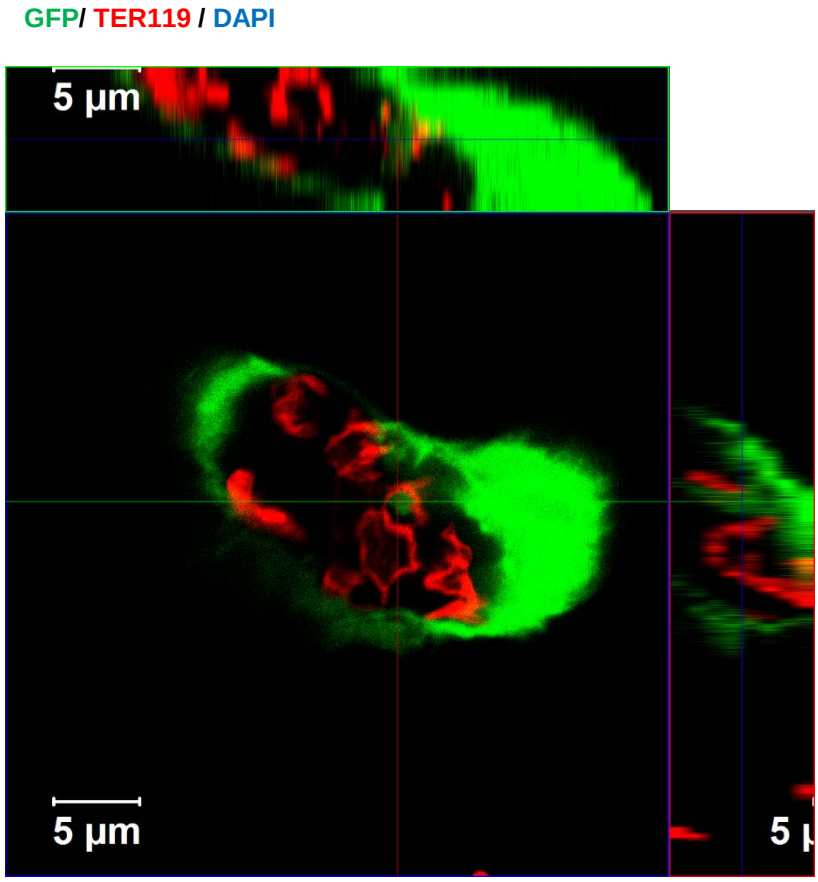

# Supplemental Figure 10

A

B

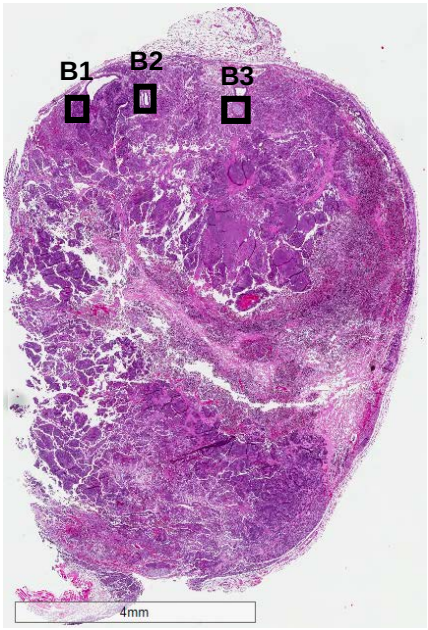


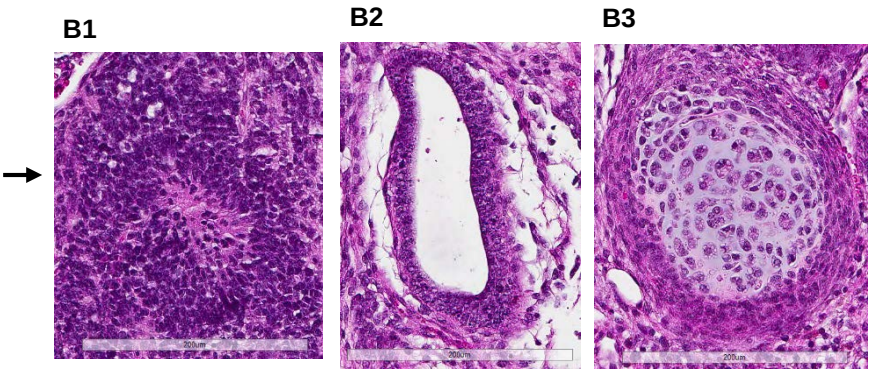


C

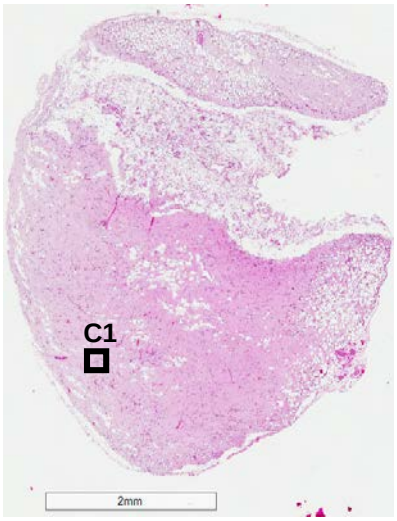


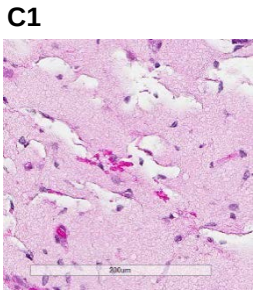


D

| | Teratoma | Non-teratoma |
|---|---|---|
| iPSCs | 5 | 0 |
| CD34$^{+}$ Progenitors | 0 | 5 |
| Fisher's exact test | P<0.01 | |

# Supplemental Figure 11

**A**

GFP / Human CD31 / Mouse CD31 / DAPI

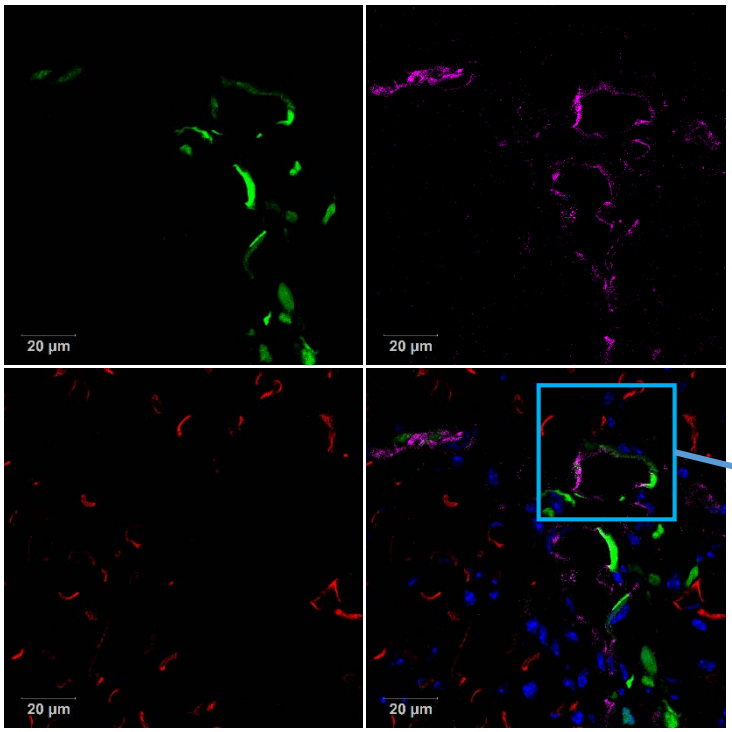


GFP / Human CD31 / Mouse CD31 / DAPI

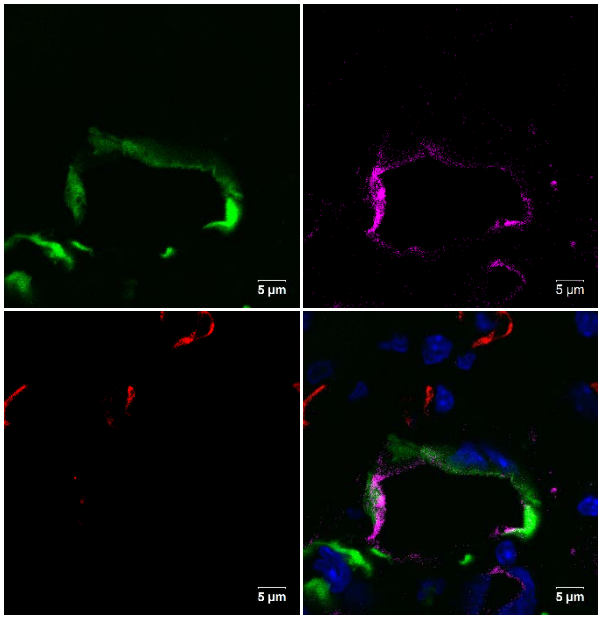


**B**

Human CD31/Mouse CD31/DAPI

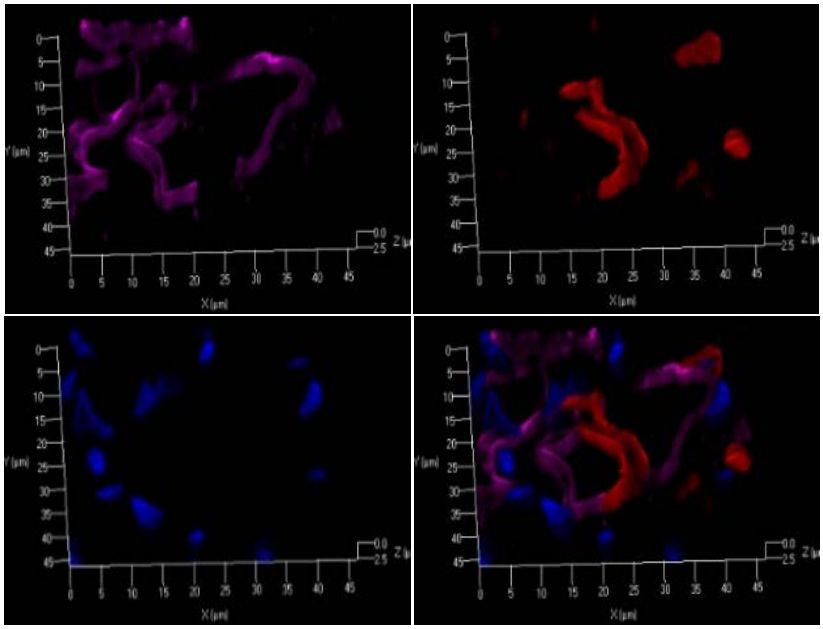

**C**

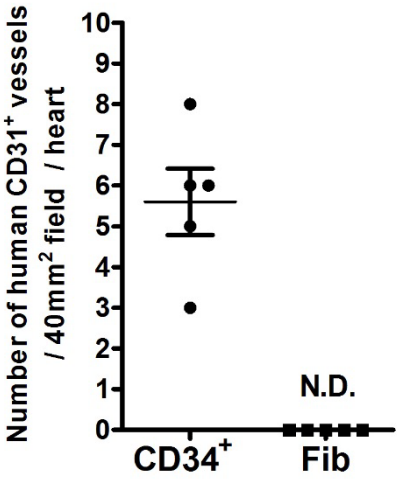

## SUPPLEMENTAL FIGURE LEGENDS

**Supplemental Figure 1.** The morphology of human adult fibroblasts (**A**), De-differentiated fibroblasts at day 7 (**B**), iECs at day 10 (**C**) and induced erythroblasts at day 4(**D**). Scale bar: 50μm for **A**, **B**, and **C**; 100μm for **D**.

**Supplemental Figure 2.** Representative flow cytometry plots (**A**), and quantification and statistical analysis (**B**) of the endothelial surface marker CD31 and VE-cadherin in fibroblasts, $CD34^+$ progenitors, and iECs at day 10, (n=3). Representative flow cytometry plots of the erythrocyte marker CD235a and mesodermal markers CD34 (**C**), and quantification and statistical analysis of $CD235a^+$ (**D**) in fibroblasts, $CD34^+$ progenitors, and iErythroblasts at day 4, (n=3). Quantification of $CD34^+$ cells in VE-$cadherin^+$ iECs at day 10 and $CD235a^+$ iErythroblasts at day 4 (n=3) (**E**). Data are presented as mean ± SE, N.S. P>0.05, ** P<0.01, *** P<0.001, using one-way ANOVA in **B** and **D**.

**Supplemental Figure 3.** Quantitative PCR analysis of endothelial specific genes - *VE-cadherin* (**A**), *CD31* (**B**), *FLK1* (**C**), and *VWF* (**D**) in $CD34^+$ progenitors, CD31 sorted iECs at day 10 and HAECs. N=3. Data are presented as mean ± SE; *P<0.05, **P<0.01, N.S., p>0.05, using one-way ANOVA.

**Supplemental Figure 4.** The time course of trans-cell electrical resistance (TER) was measured for 180 minutes in fibroblasts, human aortic endothelial cells (HAECs) and iECs. Thrombin (3.5μg/ml;0.5 unit) was added as indicated. N=3.

**Supplemental Figure 5.** Quantitative PCR analysis of *OCT4* (**A**) and *c-MYC* (**B**) in fibroblasts, $CD34^+$ progenitor cells, and iECs (at day 10), n=3. Data are presented as mean ± SE; ***P<0.001, N.S. P>0.05; compared to fibroblasts, using one-way ANONA.

**Supplemental Figure 6.** (**A**) the schematic protocol of knocking down SOX17during the induction of iECs using lentivirus expressing SOX17shRNA or retrovirus expressing Sox17. (**B**-**C**) The infection efficiency of lentivirus expressing Sox17-1 shRNA in iECs– the representative flow cytometry plot (**B**) and quantitative and statistical analysis (**C**) of GFP expression in iECs. Data are presented as mean ± SE; ***P<0.001, compared to control cells (without infection), by Student's t-test. **(D)** Immunoblots of Sox17, VE-cadherin, and CD31 in the cells infected with lentivirus expressing scramble shRNA, Sox17-1 shRNA, Sox17-2 shRNA and Sox17-3 shRNA respectively.

**Supplemental Figure 7**. Representative confocal micrographs of immunohistochemistry staining of mouse liver with anti- Mouse TER119 (red, **A**), human CD235a (red, **B**) and anti- mouse VE-cadherin (green, **A** and **B**). Nucleus stained by DAPI. Scale bars, 100μm.

**Supplemental Figure 8.** *In vivo* angiogenesis of human aortic ECs. Representative confocal micrographs of immunohistochemistry staining of plugs with anti- human CD235a (red, **A**) or anti-mouse TER119 (red, **B**) and anti- human CD31 antibodies (green, **A** & **B**). Nuclei stained by DAPI. Scale bars, 5μm.

**Supplemental Figure 9.** Representative confocal micrographs of immunohistochemistry staining of plug of GFP expressed $CD34^+$ progenitor cells (green) with anti- TER119 (red). Nucleus stained by DAPI. Scale bars, 5μm.

**Supplemental Figure 10.** *Teratoma formation*. Representative gross images (**A**) and H&E staining images of explanted plugs at 8 weeks following implantation of iPSCs (**B**) and $CD34^+$ progenitor cells (**C**). Representative H&E staining images of primitive ectodermal neuroepithelium (**B1**), endodermal epithelium (**B2**) and mesodermal cartilage (**B3**) demonstrate teratomas in plugs containing iPSCs. Representative H&E staining

images of vessels (**C1**) in the section of angiogenesis plug. **(D)** The quantification and statistical analysis of teratoma formation of $CD34^+$ progenitor cells and iPSCs (n=5) shows no teratoma formation with $CD34^+$ cells.

**Supplemental Figure 11.** Representative confocal micrographs (**A**) of immunohistochemistry staining of anti-human CD31 (magenta) and anti-mouse CD31 (red) in myocardial cross-section at two weeks post MI with GFP expressed human $CD34^+$ progenitor treatment. Scale bars, 20μm (left) and 5μm (right). Representative 3D confocal micrographs (**B**) of integration of human vessels (anti-human CD31, magenta) and mouse vessels (anti-mouse CD31, red) in heart. Nuclei stained with DAPI (blue). The quantification and statistical analysis (**C**) of human vessels (human $CD31^+$, red) formed at two weeks post-MI with human $CD34^+$ progenitors or fibroblasts (n=5) treatment in the areas receiving cell injections. Data are presented as mean ± SE. N.D., not detected.

**Supplemental Movie 1**. A representative movie shows the reconstructed 3D structure using confocal image slices, thus demonstrating the integration of human UEA I+ vessels (red) formed by GFP-labeled fibroblast-derived CD34+ progenitors with mouse host GSIB4+ vessels (far red) in an explanted Matrigel plug. Nuclei were stained with DAPI. Width of each square: 10μm.

**Supplemental Movie 2**. A representative movie shows the reconstructed 3D structure using confocal image slices, thus demonstrating the integration of human CD31+ vessels (far-red) formed by fibroblast-derived CD34+ progenitors with mouse host CD31+ vessels (red) in the heart. Nuclei were stained with DAPI. Width of each square: 2.5μm.

## References


1. Gong H, Rehman J, Tang H, Wary K, Mittal M, Chaturvedi P, Zhao YY, Komarova YA, Vogel SM and Malik AB. HIF2alpha signaling inhibits adherens junctional disruption in acute lung injury. *J Clin Invest*. 2015;125:652-64.
2. Zhang L, Malik S, Pang J, Wang H, Park KM, Yule DI, Blaxall BC and Smrcka AV. Phospholipase Cepsilon hydrolyzes perinuclear phosphatidylinositol 4-phosphate to regulate cardiac hypertrophy. *Cell*. 2013;153:216-27.
3. Tiruppathi C, Yan W, Sandoval R, Naqvi T, Pronin AN, Benovic JL and Malik AB. G protein-coupled receptor kinase-5 regulates thrombin-activated signaling in endothelial cells. *Proc Natl Acad Sci U S A*. 2000;97:7440-5.
4. Herbert BS, Hochreiter AE, Wright WE and Shay JW. Nonradioactive detection of telomerase activity using the telomeric repeat amplification protocol. *Nat Protoc*. 2006;1:1583-90.
5. Kang KT, Allen P and Bischoff J. Bioengineered human vascular networks transplanted into secondary mice reconnect with the host vasculature and re-establish perfusion. *Blood*. 2011;118:6718-21.